

- [5] X. Qu, Y. Zhai, H. Wei, C. Zhang, G. Xing, Y. Yu, F. He, Characterization and expression of three novel differentiation-related genes belong to the human NDRG gene family, *Mol. Cell. Biochem.* 229 (2002) 35–44.
- [6] V. Melotte, X. Qu, M. Ongenaert, W. van Criekinge, A.P. de Bruine, H.S. Baldwin, M. van Engeland, The N-myc downstream regulated gene (NDRG) family: Diverse functions, multiple applications, *FASEB J.* 24 (2010) 4153–4166.
- [7] M. Tepel, P. Roerig, M. Wolter, D.H. Gutmann, A. Perry, G. Reifenberger, M.J. Riemenschneider, Frequent promoter hypermethylation and transcriptional downregulation of the NDRG2 gene at 14q11.2 in primary glioblastoma, *Int. J. Cancer* 123 (2008) 2080–2086.
- [8] E.A. Lusic, M.A. Watson, M.R. Chicoine, M. Lyman, P. Roerig, G. Reifenberger, D.H. Gutmann, A. Perry, Integrative genomic analysis identifies NDRG2 as a candidate tumor suppressor gene frequently inactivated in clinically aggressive meningioma, *Cancer Res.* 65 (2005) 7121–7126.
- [9] D.C. Lee, Y.K. Kang, W.H. Kim, Y.J. Jang, D.J. Kim, I.Y. Park, B.H. Sohn, H.A. Sohn, H.G. Lee, J.S. Lim, J.W. Kim, E.Y. Song, D.M. Kim, M.N. Lee, G.T. Oh, S.J. Kim, K.C. Park, H.S. Yoo, J.Y. Choi, Y.I. Yeom, Functional and clinical evidence for NDRG2 as a candidate suppressor of liver cancer metastasis, *Cancer Res.* 68 (2008) 4210–4220.
- [10] X.L. Hu, X.P. Liu, S.X. Lin, Y.C. Deng, N. Liu, X. Li, L.B. Yao, NDRG2 expression and mutation in human liver and pancreatic cancers, *World J. Gastroenterol.* 10 (2004) 3518–3521.
- [11] H. Shi, N. Li, S. Li, C. Chen, W. Wang, C. Xu, J. Zhang, H. Jin, H. Zhang, H. Zhao, W. Song, Q. Feng, X. Feng, X. Shen, L. Yao, Q. Zhao, Expression of NDRG2 in esophageal squamous cell carcinoma, *Cancer Sci.* 101 (2010) 1292–1299.
- [12] S.C. Choi, S.R. Yoon, Y.P. Park, E.Y. Song, J.W. Kim, W.H. Kim, Y. Yang, J.S. Lim, H.G. Lee, Expression of NDRG2 is related to tumor progression and survival of gastric cancer patients through Fas-mediated cell death, *Exp. Mol. Med.* 39 (2007) 705–714.
- [13] A. Piccoli, R. Cotugno, G. Merla, A. Gentile, B. Augello, M. Quitadamo, A. Merla, A. Panza, M. Carella, R. Maglietta, A. D'Addabbo, N. Ancona, S. Fusilli, F. Perri, A. Andriulli, Promoter methylation correlates with reduced NDRG2 expression in advanced colon tumour, *BMC Med. Genomics* 2 (2009) 11.
- [14] H. Shi, H. Jin, D. Chu, W. Wang, J. Zhang, C. Chen, C. Xu, D. Fan, L. Yao, Suppression of N-myc downstream-regulated gene 2 is associated with induction of Myc in colorectal cancer and correlates closely with differentiation, *Biol. Pharm. Bull.* 32 (2009) 968–975.
- [15] H. Zhao, J. Zhang, J. Lu, X. He, C. Chen, X. Li, L. Gong, G. Bao, Q. Fu, S. Chen, W. Lin, H. Shi, J. Ma, X. Liu, Q. Ma, L. Yao, Reduced expression of N-Myc downstream-regulated gene 2 in human thyroid cancer, *BMC Cancer* 8 (2008) 303.
- [16] H. Furuta, Y. Kondō, S. Nakahata, M. Hamasaki, S. Sakoda, K. Morishita, NDRG2 is a candidate tumor-suppressor for oral squamous-cell carcinoma, *Biochem. Biophys. Res. Commun.* 391 (2010) 1785–1791.
- [17] L. Gao, G.J. Wu, X.W. Liu, R. Zhang, L. Yu, G. Zhang, F. Liu, C.G. Yu, J.L. Yuan, H. Wang, L.B. Yao, Suppression of invasion and metastasis of prostate cancer cells by overexpression of NDRG2 gene, *Cancer Lett.* 310 (2011) 94–100.
- [18] S.P. Song, S.B. Zhang, R. Liu, L. Yao, Y.Q. Hao, M.M. Liao, Y.D. Zhang, Z.H. Li, NDRG2 down-regulation and CD24 up-regulation promote tumor aggravation and poor survival in patients with gallbladder carcinoma, *Med. Oncol.* 29 (2012) 1879–1885.
- [19] M.P. Tschan, D. Shan, J. Laedrach, M. Eyholzer, E.O. Leibundgut, G.M. Baerlocher, A. Tobler, D. Stroka, M.F. Fey, NDRG1/2 expression is inhibited in primary acute myeloid leukemia, *Leuk. Res.* 34 (2010) 393–398.
- [20] S.J. Li, W.Y. Wang, B. Li, B. Chen, B. Zhang, X. Wang, C.S. Chen, Q.C. Zhao, H. Shi, L. Yao, Expression of NDRG2 in human lung cancer and its correlation with prognosis, *Med. Oncol.* 30 (2013) 421.
- [21] N. Liu, L. Wang, X. Li, Q. Yang, X. Liu, J. Zhang, Y. Wu, S. Ji, Y. Zhang, A. Yang, H. Han, L. Yao, N-Myc downstream-regulated gene 2 is involved in p53-mediated apoptosis, *Nucleic Acids Res.* 36 (2008) 5335–5349.
- [22] A. Kim, M.J. Kim, Y. Yang, J.W. Kim, Y.I. Yeom, J.S. Lim, Suppression of NF-kappaB activity by NDRG2 expression attenuates the invasive potential of highly malignant tumor cells, *Carcinogenesis* 30 (2009) 927–936.
- [23] N. Liu, L. Wang, X. Liu, Q. Yang, J. Zhang, W. Zhang, Y. Wu, L. Shen, Y. Zhang, A. Yang, H. Han, L. Yao, Promoter methylation, mutation, and genomic deletion are involved in the decreased NDRG2 expression levels in several cancer cell lines, *Biochem. Biophys. Res. Commun.* 358 (2007) 164–169.
- [24] J. Zhang, F. Li, X. Liu, L. Shen, J. Liu, J. Su, W. Zhang, Y. Deng, L. Wang, N. Liu, W. Han, S. Ji, A. Yang, H. Han, L. Yao, The repression of human differentiation-related gene NDRG2 expression by Myc via Miz-1-dependent interaction with the NDRG2 core promoter, *J. Biol. Chem.* 281 (2006) 39159–39168.
- [25] International Union Against Cancer (UICC), TNM Classification of Malignant Tumor, sixth ed., Wiley-Liss, New York, 2002.
- [26] T. Furukawa, M. Sunamura, F. Motoi, S. Matsuno, A. Horii, Potential tumor suppressive pathway involving DUSP6/MKP-3 in pancreatic cancer, *Am. J. Pathol.* 162 (2003) 1807–1815.
- [27] H. Sasaki, K. Miura, A. Horii, N. Kaneko, W. Fujibuchi, L. Kiseleva, Z. Gu, Y. Murata, H. Karasawa, T. Mizoi, T. Kobayashi, M. Kinouchi, S. Ohnuma, N. Yazaki, M. Unno, I. Sasaki, Orthotopic implantation mouse model and cDNA microarray analysis indicates several genes potentially involved in lymph node metastasis of colorectal cancer, *Cancer Sci.* 99 (2008) 711–719.
- [28] T. Tabata, N. Tsukamoto, A.A. Fooladi, S. Yamanaka, T. Furukawa, M. Ishida, D. Sato, Z. Gu, H. Nagase, S. Egawa, M. Sunamura, A. Horii, RNA interference targeting against S100A4 suppresses cell growth and motility and induces apoptosis in human pancreatic cancer cells, *Biochem. Biophys. Res. Commun.* 390 (2009) 475–480.
- [29] K. Ogawa, K. Shiga, S. Saijo, T. Ogawa, N. Kimura, A. Horii, A novel G106D alteration of the SDHD gene in a pedigree with familial paraganglioma, *Am. J. Med. Genet. A.* 140 (2006) 2441–2446.
- [30] N. Kaneko, K. Miura, Z. Gu, H. Karasawa, S. Ohnuma, H. Sasaki, N. Tsukamoto, S. Yokoyama, A. Yamamura, H. Nagase, C. Shibata, I. Sasaki, A. Horii, siRNA-mediated knockdown against CDCA1 and KNTC2, both frequently overexpressed in colorectal and gastric cancers, suppresses cell proliferation and induces apoptosis, *Biochem. Biophys. Res. Commun.* 390 (2009) 1235–1240.
- [31] M. Sato, Y. Mori, A. Sakurada, S. Fujimura, A. Horii, The H-cadherin (CDH13) gene is inactivated in human lung cancer, *Hum. Genet.* 103 (1998) 96–101.
- [32] J.P. Neoptolemos, D.D. Stocken, C. Bassi, P. Ghaneh, D. Cunningham, D. Goldstein, R. Padbury, M.J. Moore, S. Gallinger, C. Mariette, M.N. Wente, J.R. Izbicki, H. Friess, M.M. Lerch, C. Dervenis, A. Olah, G. Butturini, R. Doi, P.A. Lind, D. Smith, J.W. Valle, D.H. Palmer, J.A. Buckels, J. Thompson, C.J. McKay, C.L. Rawcliffe, M.W. Buchler, European study group for pancreatic, ADJUVANT chemotherapy with fluorouracil plus folinic acid vs gemcitabine following pancreatic cancer resection: a randomized controlled trial, *JAMA* 304 (2010) 1073–1081.
- [33] K.N. Bhalla, Epigenetic and chromatin modifiers as targeted therapy of hematologic malignancies, *J. Clin. Oncol.* 23 (2005) 3971–3993.
- [34] M. Haberland, R.L. Montgomery, E.N. Olson, The many roles of histone deacetylases in development and physiology: implications for disease and therapy, *Nat. Rev. Genet.* 10 (2009) 32–42.
- [35] S. Thiagalingam, K.H. Cheng, H.J. Lee, N. Mineva, A. Thiagalingam, J.F. Ponte, Histone deacetylases: unique players in shaping the epigenetic histone code, *Ann. N.Y. Acad. Sci.* 983 (2003) 84–100.
- [36] K. Miyake, T. Yoshizumi, S. Imura, K. Sugimoto, E. Batmunkh, H. Kanemura, Y. Morine, M. Shimada, Expression of hypoxia-inducible factor-1alpha, histone deacetylase 1, and metastasis-associated protein 1 in pancreatic carcinoma: correlation with poor prognosis with possible regulation, *Pancreas* 36 (2008) e1–e9.
- [37] G. Wang, J. He, J. Zhao, W. Yun, C. Xie, J.W. Taub, A. Azmi, R.M. Mohammad, Y. Dong, W. Kong, Y. Guo, Y. Ge, Class I and Class II histone deacetylases are potential therapeutic targets for treating pancreatic cancer, *PLoS ONE* 7 (2012) e52095.
- [38] G. Schneider, O.H. Kramer, P. Fritsche, S. Schuler, R.M. Schmid, D. Saur, Targeting histone deacetylases in pancreatic ductal adenocarcinoma, *J. Cell Mol. Med.* 14 (2010) 1255–1263.
- [39] M. Dokmanovic, C. Clarke, P.A. Marks, Histone deacetylase inhibitors: overview and perspectives, *Mol. Cancer Res.* 5 (2007) 981–989.
- [40] M. New, H. Olzsha, N.B. La Thangue, HDAC inhibitor-based therapies: can we interpret the code?, *Mol. Oncol.* 6 (2012) 637–656.
- [41] D.I. Dovzhanskiy, S.M. Arnold, T. Hackert, I. Oehme, O. Witr, K. Felix, N. Giese, J. Werner, Experimental in vivo and in vitro treatment with a new histone deacetylase inhibitor belinostat inhibits the growth of pancreatic cancer, *BMC Cancer* 12 (2012) 226.
- [42] M. Donadelli, C. Costanzo, L. Faggioli, M.T. Scupoli, P.S. Moore, C. Bassi, A. Scarpa, M. Palmieri, Trichostatin A, an inhibitor of histone deacetylases, strongly suppresses growth of pancreatic adenocarcinoma cells, *Mol. Carcinog.* 38 (2003) 59–69.
- [43] J. Bai, A. Demirjian, J. Sui, W. Marasco, M.P. Callery, Histone deacetylase inhibitor trichostatin A and proteasome inhibitor PS-341 synergistically induce apoptosis in pancreatic cancer cells, *Biochem. Biophys. Res. Commun.* 348 (2006) 1245–1253.

## ORIGINAL ARTICLE

# Oral administration of an HSP90 inhibitor, 17-DMAG, intervenes tumor-cell infiltration into multiple organs and improves survival period for ATL model mice

E Ikebe<sup>1</sup>, A Kawaguchi<sup>2,3,13</sup>, K Tezuka<sup>4,13</sup>, S Taguchi<sup>1,13</sup>, S Hirose<sup>1</sup>, T Matsumoto<sup>1</sup>, T Mitsui<sup>1</sup>, K Senba<sup>1</sup>, A Nishizono<sup>1</sup>, M Hori<sup>5</sup>, H Hasegawa<sup>6</sup>, Y Yamada<sup>6</sup>, T Ueno<sup>4</sup>, Y Tanaka<sup>7</sup>, H Sawa<sup>3</sup>, W Hall<sup>8</sup>, Y Minami<sup>9</sup>, KT Jeang<sup>10</sup>, M Ogata<sup>11</sup>, K Morishita<sup>12</sup>, H Hasegawa<sup>2</sup>, J Fujisawa<sup>4</sup> and H Iha<sup>1</sup>

In the peripheral blood leukocytes (PBLs) from the carriers of the human T-lymphotropic virus type-1 (HTLV-1) or the patients with adult T-cell leukemia (ATL), nuclear factor kappaB (NF- $\kappa$ B)-mediated antiapoptotic signals are constitutively activated primarily by the HTLV-1-encoded oncoprotein Tax. Tax interacts with the I  $\kappa$ B kinase regulatory subunit NEMO (NF- $\kappa$ B essential modulator) to activate NF- $\kappa$ B, and this interaction is maintained in part by a molecular chaperone, heat-shock protein 90 (HSP90), and its co-chaperone cell division cycle 37 (CDC37). The antibiotic geldanamycin (GA) inhibits HSP90's ATP binding for its proper interaction with client proteins. Administration of a novel water-soluble and less toxic GA derivative, 17-dimethylaminoethylamino-17-demethoxygeldanamycin hydrochloride (17-DMAG), to Tax-expressing ATL-transformed cell lines, C8166 and MT4, induced significant degradation of Tax. 17-DMAG also facilitated growth arrest and cellular apoptosis to C8166 and MT4 and other ATL cell lines, although this treatment has no apparent effects on normal PBLs. 17-DMAG also downregulated Tax-mediated intracellular signals including the activation of NF- $\kappa$ B, activator protein 1 or HTLV-1 long terminal repeat in Tax-transfected HEK293 cells. Oral administration of 17-DMAG to ATL model mice xenografted with lymphomatous transgenic Lck-Tax (Lck proximal promoter-driven Tax transgene) cells or HTLV-1-producing tumor cells dramatically attenuated aggressive infiltration into multiple organs, inhibited *de novo* viral production and improved survival period. These observations identified 17-DMAG as a promising candidate for the prevention of ATL progression.

*Blood Cancer Journal* (2013) 3, e132; doi:10.1038/bcj.2013.30; published online 16 August 2013

**Keywords:** 17-DMAG; molecular chaperon; Tax; ATL; apoptosis; transgenic model

## INTRODUCTION

Nuclear factor kappaB (NF- $\kappa$ B) is a transcription factor that regulates immune and antiapoptotic responses to multiple extracellular stresses.<sup>1,2</sup> Under normal conditions, most NF- $\kappa$ B molecules are sequestered in the cytoplasm by the inhibitor I  $\kappa$ B. In response to cellular stress, I  $\kappa$ B is rapidly phosphorylated by the NF- $\kappa$ B activator I  $\kappa$ B kinase (IKK) and ubiquitylated for degradation by the proteasome. This frees NF- $\kappa$ B for translocation into the nucleus, where it directs the transcriptional activation of NF- $\kappa$ B-responsive genes.<sup>3,4</sup> IKK is comprised of three different subunits, IKK $\alpha$ , IKK $\beta$  and IKK $\gamma$ /NEMO (NF- $\kappa$ B essential modulator). IKK $\gamma$  is also known as NF- $\kappa$ B essential modulator (NEMO). NEMO trimerizes rapidly in response to extracellular stimuli, such as the pro-inflammatory cytokine tumor necrosis factor- $\alpha$  (TNF- $\alpha$ ), and recruits the two catalytic subunits, IKK $\alpha$ / $\beta$ , to form a highly phosphorylated active IKK holoenzyme.<sup>5</sup> Several genetic studies have shown that cytokine-triggered activation of what is

termed the canonical NF- $\kappa$ B activation pathway is primarily dependent on NEMO and IKK $\beta$ ,<sup>6,7</sup> whereas IKK $\alpha$  activity is required for the development of the skin, limbs and lymph nodes.<sup>8,9</sup> Upon stimulation, several accessory proteins are recruited to IKK, and the molecular size of this active IKK complex reaches more than 1MDa.<sup>10,11</sup> The molecular chaperone heat-shock protein 90 (HSP90) and its co-chaperone cell division cycle 37 (CDC37) are components of this high molecular weight (HMW)-IKK complex, and they play crucial roles in maintaining the activity of the complex.<sup>12</sup> The antibiotic geldanamycin (GA) specifically binds to the ATPase domain of HSP90 and inhibits its function as a molecular chaperone, resulting in the efficient inhibition of TNF- $\alpha$ -mediated activation of NF- $\kappa$ B.<sup>12,13</sup>

The human T-lymphotropic virus type-1 (HTLV-1), which is the etiologic agent of adult T-cell leukemia (ATL), encodes the oncoprotein Tax.<sup>14–16</sup> Tax activates NF- $\kappa$ B by interacting

<sup>1</sup>Department of Infectious Diseases, Faculty of Medicine, Oita University, Yufu, Japan; <sup>2</sup>Department of Pathology, National Institute of Infectious Diseases, Musashimurayama, Japan; <sup>3</sup>Department of Molecular Pathobiology, 21st Century COE Program for Zoonosis Control, Hokkaido University Research Center for Zoonosis Control, Sapporo, Japan; <sup>4</sup>Department of Microbiology, Kansai Medical University, Moriguchi, Japan; <sup>5</sup>Department of Hematology, Ibaraki Prefectural Central Hospital, Kasama, Ibaraki, Japan; <sup>6</sup>Department of Laboratory Medicine, Nagasaki University Graduate School of Biomedical Sciences, Nagasaki, Japan; <sup>7</sup>Department of Immunology, Graduate School of Medicine, University of the Ryukyus, Nishihara, Japan; <sup>8</sup>Department of Medical Microbiology, Centre for Research in Infectious Diseases, Conway Institute of Biomolecular and Biomedical Research, University College Dublin, Dublin, Ireland; <sup>9</sup>Department of Biotechnology, Maebashi Institute of Technology, Maebashi, Japan; <sup>10</sup>Molecular Virology Section, Laboratory of Molecular Microbiology, National Institute of Allergy and Infectious Diseases, Bethesda, MD, USA; <sup>11</sup>Department of Hematology, Faculty of Medicine, Oita University, Yufu, Japan and <sup>12</sup>Division of Tumor and Cellular Biochemistry, Department of Medical Sciences, Faculty of Medicine, University of Miyazaki, Miyazaki, Japan. Correspondence: Dr H Iha, Department of Infectious Diseases, Faculty of Medicine, Oita University, 1-1 Iidaigaoka, Hasama, Yufu, Oita 879-5593, Japan. E-mail: hiha@oita-u.ac.jp

<sup>13</sup>These authors contributed equally to this work.

Received 25 June 2012; revised 24 June 2013; accepted 28 June 2013

physically with NEMO.<sup>10,17</sup> NF- $\kappa$ B activation mediated by this Tax-NEMO interaction is similar to that of the TNF- $\alpha$ -triggered 'canonical' pathway. Tax induces IKK phosphorylation, ubiquitylation and proteasome-dependent degradation of I  $\kappa$ B, thereby inducing the translocation of NF- $\kappa$ B into the nucleus.<sup>18,19</sup> However, in contrast to the TNF- $\alpha$ -triggered canonical pathway, which is transient and mostly IKK $\beta$  dependent, Tax-mediated NF- $\kappa$ B activation is persistent and utilizes both the IKK $\alpha$  and IKK $\beta$  subunits.<sup>20,21</sup> From these observations, we speculated that oncogenic Tax-mediated activation of NF- $\kappa$ B is distinguishable from the canonical NF- $\kappa$ B activation pathway, and indeed, we have succeeded in inhibiting Tax-mediated NF- $\kappa$ B activation using selected sets of NEMO-mutant peptides.<sup>11</sup>

Those earlier studies led us to ask whether GA can inhibit Tax-mediated HMW-IKK formation and suppress NF- $\kappa$ B activation as has been demonstrated in the TNF- $\alpha$ -triggered canonical pathway. To address this, we treated ATL cell lines or HEK293 cells transfected with a Tax expression vector with GA or its less toxic derivative 17-dimethylaminoethylamino-17-démethoxygeldanamycin hydrochloride (17-DMAG).<sup>22</sup> We found that these HSP90 inhibitors downregulated Tax-mediated intracellular activity including the activation of NF- $\kappa$ B, activator protein 1 and HTLV-1 long terminal repeat (HTLV-1-LTR). These findings prompted us to investigate the molecular mechanisms by which HSP90 inhibitors disrupt Tax-mediated signaling in ATL cells. We found that the stability of Tax in ATL cells is heavily dependent on the HSP90/CDC37 chaperones and that Tax is rapidly degraded without these chaperones following the addition of HSP90 inhibitors. Apoptosis of ATL cells was also induced by GA and 17-DMAG. Finally, the oral administration of 17-DMAG to severe combined immunodeficient (SCID) mice transplanted with lymphomatous cells bearing Lck proximal promoter-driven Tax transgene (Lck-Tax) cells<sup>23</sup> markedly inhibited the aggressive infiltration of these Lck-Tax cells into multiple organs. The same procedure to the humanized NOG (huNOG) mice inoculated with HTLV-1-producing Jurkat cells also resulted in the suppression of *de novo* viral production and improved the survival period.

## MATERIALS AND METHODS

### Ethics statement

This study was carried out in strict accordance with the recommendations in the Guidelines for Proper Conduct of Animal Experiments, Science Council of Japan (<http://www.scj.go.jp/en/animal/index.html>). All procedures involving animals and their care were approved by the Animal Care Committee of Oita University, National Institute of Infectious Diseases and Kansai Medical University in accordance with the Regulations for Animal Experiments in Oita University (approval ID: 24-22).

### Chemicals, cells and cell culture conditions

All chemicals used in this study including 17-DMAG<sup>22</sup> and cell lines or peripheral blood leukocytes (PBLs) were described in Supplementary Information.

### Coimmunoprecipitation and immunoblot

One million cells of MT4 and C8166 treated with or without 17-DMAG and HEK293 cells transfected with each plasmid (maximum 1  $\mu$ g) by EugeneHD (Roche Applied Science, Tokyo, Japan) for 40 h were lysed with coimmunoprecipitation (Co-IP) buffer. Each 200  $\mu$ g of precleared (with 30  $\mu$ l of protein G agarose, CalBiochem, Millipore Corporation, Billerica, MA, USA) lysates was incubated with 2  $\mu$ g of rabbit polyclonal anti-HSP90 (Stressgen Bioreagents, Ann Arbor, MI, USA) or rabbit anti-FLAG antibody (Sigma-Aldrich, St Louis, MO, USA) for at least 3 h at 4°C. Antibody-protein G complexes were washed, resolved by sodium dodecyl sulfate-polyacrylamide gel electrophoresis and transferred onto a polyvinylidene difluoride membrane, and specific proteins were detected by monoclonal anti-Tax, -HSP90 (Stressgen), -Flag, -tubulin (Sigma) or polyclonal anti-IKK $\beta$  (Cell Signaling Technology) antibodies, respectively.

### Real-time quantitative reverse transcriptase-PCR by the LightCycler system

Total RNA from MT4 cells treated with or without 17-DMAG was isolated using ISOGEN (Wako Pure Chemical Industries, Ltd., Osaka, Japan), and contaminated DNA was removed. cDNA was constructed by the Thermo-script reverse transcriptase-PCR system (Invitrogen, Life Technologies Japan Co., Tokyo, Japan), and real-time quantitative PCRs for Tax and glucose-6-phosphate 1-dehydrogenase were performed on a Roche LC480 system (Roche) with indicated probe and primer sets.

### Cell viability assay

Cell lines or PBLs from ATL patients or healthy donors were treated with 2.5  $\mu$ M of 17-DMAG for 1–4 days. After every 24 h incubation, cell viabilities were counted with Cell Counting Kit (Dojindo Laboratories, Kumamoto, Japan).

### Caspase-3/7 assay

Cells used in the 'cell viability assay' were also subjected for apoptosis activity with caspase-3/7 assay and GLOMAX 96 microplate luminometer (Promega KK, Tokyo, Japan).

### Plasmids

The details of plasmid pSG5-Tax,<sup>24</sup> HSP90,<sup>25</sup> Cdc37,<sup>26</sup> CMV-Tax or LTR-Tax<sup>11</sup> and CoralHue-Tax or -CDC37 vectors (MBL Co. Ltd., Nagoya, Japan)<sup>27</sup> are described in Supplementary Information.

### Luciferase assay

HEK293 cells were transfected with plasmid DNA mixture containing the reporter plasmids (NF- $\kappa$ B-Luc or HTLV-1-LTR-Luc<sup>11</sup> and RSV- $\beta$ -galactosidase as a transfection indicator) and Tax expression vectors (pSG5-Tax, CMV-Tax or LTR-Tax) by EugeneHD. After 24 h incubation of the transfection, where indicated, 17-DMAG at concentrations listed in the figures was added, and cells were further incubated for 16 h. Cell lysates were subjected to the luciferase assay kit and GLOMAX 96.

### Microscopic observation of cells

HEK293 cells were transfected with phmKGN-MC-Tax and phmKGC-MN-Cdc37 or its mutant -Cdc37(N200) or -Cdc37(N180) for 48 h and then treated with 1  $\mu$ M of Hoechst 34442 (Sigma). Light and fluorescent (green fluorescent protein (GFP) or Hoechst 34442) microscopic observation and photography were performed by BZ-9000 Biorevo (Keyence Co. Ltd., Osaka, Japan).

### Transfer of Lck-Tax transgenic cells to SCID mice and treatment with 17-DMAG

SCID mice were injected intraperitoneally with  $2 \times 10^6$  Lck-Tax cells.<sup>23</sup> 17-DMAG was administered orally 5 days per week, with 5, 15 or 30 mg/kg for 2–3 weeks, and then mice were sacrificed for pathological examination.

### HTLV-1 infection to huNOG and flow cytometric analysis of peripheral bloods

Suspension of irradiated  $1 \times 10^6$  HTLV-1-producing JEX cells was inoculated intraperitoneally into huNOG mice<sup>28</sup> at the age between 24 and 28 weeks. Peripheral blood cells were routinely collected every 2 weeks after infection. Spleen, bone marrow and lymph node were collected, and PBLs were stained with fluorescent dye-conjugated antibodies against human cellular surface markers.

### DNA isolation and quantification of proviral load

Genomic DNA was extracted from single cell suspension of tissue or peripheral blood followed by the conventional phenol extraction method. Proviral load was measured by quantitative PCR as previously described.<sup>29</sup>

### Histopathological examination and immunohistochemistry

Tissues were directly fixed in the neutral buffered formalin (Sigma), embedded in paraffin, sectioned and stained with hematoxylin and eosin. Peripheral blood smears were prepared using Giemsa staining and examined by light microscopy.

For details, see Supplementary Information.

**RESULTS**

The NF- $\kappa$ B-activating Tax-HSP90-IKK ternary complex is disaggregated by HSP90 inhibitors that induce Tax degradation. The molecular chaperone HSP90 and its co-chaperone CDC37 are both recruited to IKK and play essential roles in TNF- $\alpha$ -triggered HMW-IKK formation and subsequent NF- $\kappa$ B activation. The addition of the HSP90-specific inhibitor GA completely suppresses NF- $\kappa$ B signaling.<sup>12</sup> As we previously demonstrated that the expression of Tax also resulted in the formation of a HMW-IKK complex for activating NF- $\kappa$ B,<sup>11</sup> we speculated that the inhibition of HSP90 function by GA would also affect Tax-mediated NF- $\kappa$ B signaling. First, using Tax-expressing MT4 cells, we confirmed the interaction of Tax with HSP90 in the same protein complex by Co-IP assays (Figure 1a). We then treated MT4 cells for 24 h with a newly developed, less toxic and water-soluble GA derivative, 17-DMAG,<sup>22</sup> to evaluate its effects on the formation of a Tax-induced ternary complex, Tax-HSP90-IKK. To our surprise, the amount of Tax in MT4 cells decreased progressively with increasing doses of 17-DMAG (Figure 1b, upper panel) despite no apparent changes in the amount of HSP90 in the same lysate (data not shown). Under these conditions, the interaction between HSP90 and IKK $\beta$  was clearly reduced with increasing doses of 17-DMAG (Figure 1b, middle panel), whereas the amount of HSP90 immunoprecipitated throughout this range of concentrations was unchanged (Figure 1b, lower panel).

We then examined the kinetics of Tax degradation in MT4 cells treated with 17-DMAG. Reductions in Tax levels were observed in cells treated for 12 h and continued over time until by 48 h, when the level of Tax became undetectable (Figure 1c). This

17-DMAG-induced Tax degradation stabilized I  $\kappa$ B $\alpha$ , whereas another NF- $\kappa$ B inhibitor dexamethasone had no effects (Supplementary Figure 1). Tax degradation by 17-DMAG occurred prior to mRNA suppression as the marked decrease of Tax mRNA was not observed until 24 h after treatment (Figure 1d), whereas protein level of Tax was obviously decreased by 12 h (compare Figures 1c and d). Our previous study indicated that Tax degradation is partly induced by caspase,<sup>30</sup> and polyubiquitylation had little effects on its cellular stability.<sup>31</sup> We therefore re-evaluated which pathway is responsible for the 17-DMAG-induced Tax degradation (Figure 1e). Tax degradation was partly blocked by the caspase inhibitor zVAD-fmk<sup>30</sup> and by autophagy inhibitors 3-methyladenine (3-MA) and 5-aminoimidazole-4-carboxamide-1- $\beta$ -D-ribofuranoside (AICAR)<sup>32</sup> but not by the proteasome inhibitor MG132. Similar findings were obtained from parallel studies using another ATL cell line, C8166 (data not shown), although more investigation is needed for fully understanding of Tax instability.

GA and its derivatives are known to suppress a variety of intracellular signaling pathways, including NF- $\kappa$ B activation by inhibiting IKK.<sup>12,33</sup> One of the most important functions of NF- $\kappa$ B is to protect cells from apoptotic stress. A portion of 2.5  $\mu$ M of 17-DMAG is sufficient to induce Tax degradation (Figure 1c) and I  $\kappa$ B $\alpha$  stabilization (Supplementary Figure 1), which implies the suppression of ATL cell growth; however, it is important to know whether this concentration is toxic to normal PBLs. We, therefore, confirmed the median inhibitory concentrations of 17-DMAG for several ATL or non-ATL cell lines along with normal PBLs.

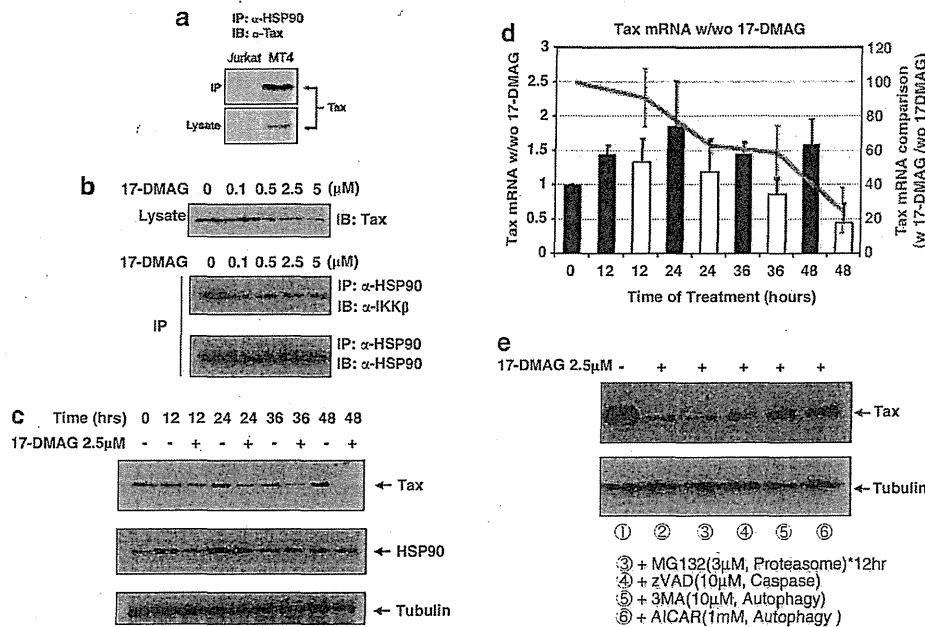


**Figure 1.** 17-DMAG inhibits HSP90-Tax-IKK ternary complex formation and induces Tax degradation in ATL cells. (a) Co-IP of Tax and HSP90. Four million Jurkat or MT4 cells were lysed with Co-IP buffer, and 50  $\mu$ g total of cell lysates were subjected to IP with 2  $\mu$ g of rabbit polyclonal anti-HSP90 antibody, followed by immunoblot (IB) with mouse monoclonal anti-Tax antibody (upper panel). The amount of expressed Tax in each cell line was verified by IB with anti-Tax against 10  $\mu$ g of cell lysates (lower panel). (b) 17-DMAG's effects on Tax expression level and physical interaction between HSP90 and IKK $\beta$  in MT4 cells. Four million MT4 cells were treated with the indicated concentrations of 17-DMAG for 16 h. Co-IP and IB against immunoprecipitates or lysates were carried out as in panel a. (c) Ten micrograms of each cell lysate from MT4 cells treated with or without 2.5  $\mu$ M of 17-DMAG for the indicated periods were subjected to sodium dodecyl sulfate-polyacrylamide gel electrophoresis, and Tax (upper panel), HSP90 (middle panel) or tubulin (lower panel) expression was detected using monoclonal anti-Tax, anti-HSP90 or anti-tubulin antibodies. (d) Expression levels of Tax in 17-DMAG-treated MT4 cells. mRNAs were prepared from the same aliquots of MT4 cells described in panel c. mRNAs from 17-DMAG-untreated fractions (black bars) and 17-DMAG-treated fractions (2.5  $\mu$ M, white bars) with indicated time courses were analyzed with the universal probes (Roche) and primers through the LightCycler PCR method according to the manufacturer's direction. Comparison of Tax mRNAs with or without 17-DMAG was also indicated with a red line graph as a division of Tax mRNA with 17-DMAG/without 17-DMAG at each time point. (e) Four million MT4 cells were treated with 2.5  $\mu$ M 17-DMAG for 24 h (lanes 2-6) and then additional 3  $\mu$ M MG132 for 12 h (lane 3), 10  $\mu$ M zVAD-fmk (lane 4) and 3-MA (lane 5) and 1 mM AICAR (lane 6) for 24 h. Lysates were prepared for IB of Tax and tubulin.

The median inhibitory concentrations to ATL cells vary from 0.06 to 2.33  $\mu\text{M}$ , which is much lower than that of non-ATL Jurkat cells (9.32  $\mu\text{M}$ ), and three PBLs did not show any significant growth suppression with 10  $\mu\text{M}$  of 17-DMAG (Supplementary Figure 2). We set the concentration of 17-DMAG at 2.5  $\mu\text{M}$  and measured the effects on the viability of ATL cells (cell lines established from ATL patients' PBLs or cord blood cocultured with ATL patients' PBLs or primary PBLs of ATL patients) and other leukemic cells, as well as PBLs from HTLV-1-negative controls. Most of the ATL cell lines treated with 17-DMAG exhibited a rapid decrease in viability,

whereas normal PBLs were unaffected by the drug (Figure 2a). 17-DMAG treatment also resulted in a marked increase in caspase-3/7 activity in most of the ATL cell lines while having no significant caspase perturbation in control PBLs (Figure 2b).

Downregulation of Tax occurs at the post-transcriptional stage  
We then proceeded to examine the details of 17-DMAG-dependent inhibitory effects on the Tax-HSP90- $\text{IKK}$  ternary complex by transfection of two different Tax expression vectors into HEK293 cells. One was driven by the simian virus 40 early promoter and

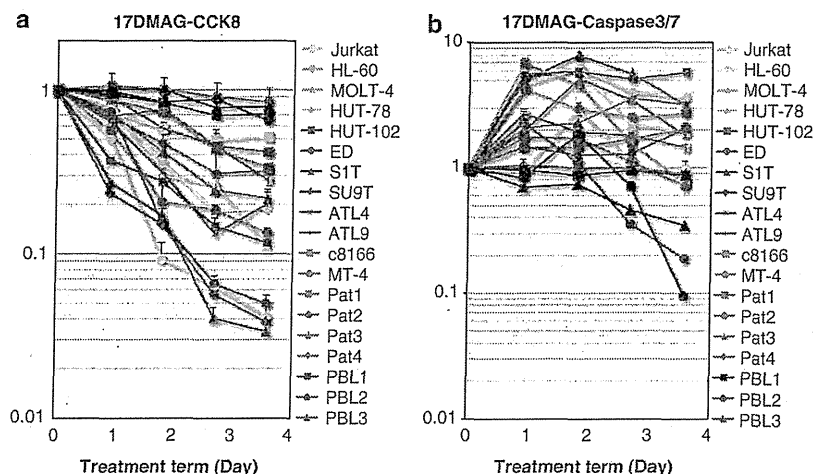


**Figure 2.** 17-DMAG induces growth arrest and apoptosis in ATL cells. Two million cells from each ATL cell line established from ATL patients' PBLs (HUT-102, ED, S1T, SU9T, ATL4 and ATL9; red lines), ATL cell lines established by coculture of cord blood and ATL patients' PBLs (C8166 and MT4; orange lines), PBLs from ATL patients (Pat1 to Pat4; purple lines), non-ATL leukemic cell lines (Jurkat, HL-60, MOLT-4 and HUT-78; yellow lines) or healthy donors (PBL1, PBL2 and PBL3; blue lines) were treated with 2.5  $\mu\text{M}$  of 17-DMAG for 1–4 days. After each 24 h incubation,  $10^4$  (a) or  $5 \times 10^3$  (b) cells were transferred to each well of a 96-well plate. (a) One-tenth volume of Cell Counting Kit 8 solution (Dojindo) was added to each fraction. Thirty minutes after incubation, the absorbance at 465 nm was measured using an E-max precision microplate reader (Molecular Devices Japan Co. Ltd., Tokyo, Japan). (b) The same volume of Apo-ONE homogeneous Caspase-3/7 assay solution was added to cells, and chemical luminescence was quantified with GloMax luminometer (Promega).

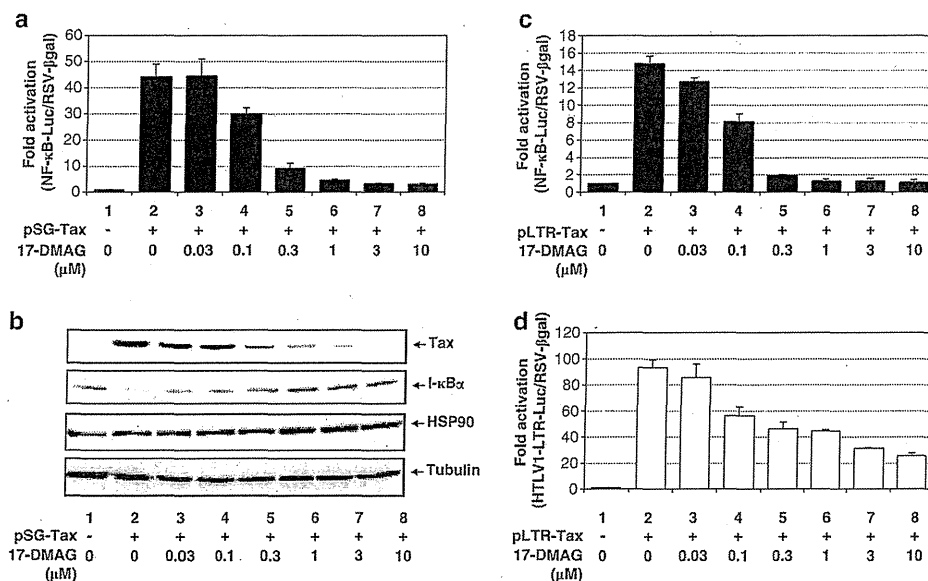


**Figure 3.** 17-DMAG downregulates all the Tax-mediated signaling in HEK293 cells. Fifty thousand HEK293 cells in each well on a 12-well plate were transfected with 0.5  $\mu\text{g}$  of pSG-Tax (a, c) or pLTR-Tax along with 50 ng of NF- $\kappa\text{B}$ -luciferase (a, c) or HTLV-1-LTR-luciferase (d) and 50 ng of RSV- $\beta$ -galactosidase control plasmid. A portion of 0.1–5  $\mu\text{M}$  of 17-DMAG was added as indicated for 16 h. (b) The expression levels of Tax, HSP90 and tubulin in 10  $\mu\text{g}$  of lysates from panel (a) were monitored by IB with monoclonal antibodies for each protein.

$\beta$ -globin intron II (pSG5-Tax),<sup>24</sup> whereas the other was driven by the HTLV-1-LTR (LTR-Tax). These lines were transfected with either a NF- $\kappa$ B-responsive or a HTLV-1-LTR luciferase reporter (Figures 3a and b and Figures 3c and d, respectively) and RSV- $\beta$ -galactosidase for readout normalization. 17-DMAG treatment was found to suppress Tax-mediated NF- $\kappa$ B (Figures 3a, b and c) or HTLV-1-LTR activation (Figure 3d) regardless of whether Tax was expressed from

pSG5-Tax (Figures 3a and b) or LTR-Tax (Figures 3c and d). In these experiments, the ectopically expressed Tax from transfected plasmid was again downregulated by 17-DMAG (Figure 3b). The same results were also obtained from the cell lysates transfected with LTR-Tax or CMV-Tax (data not shown). In addition to these two enhancers, activator protein 1 activation by Tax<sup>34</sup> was also inhibited by 17-DMAG (data not shown). As the three discrete pathways

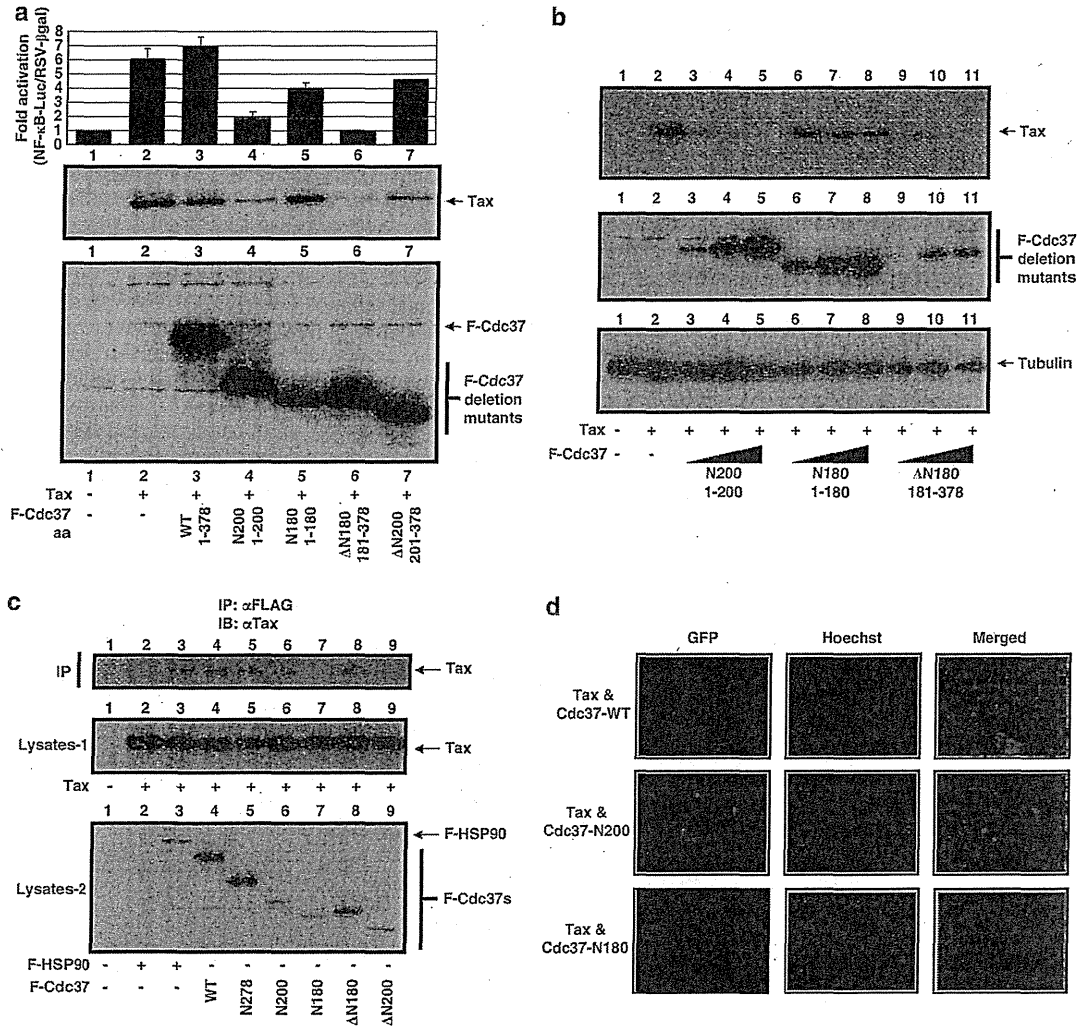


**Figure 4.** CBD of Cdc37 plays a crucial role for Tax stability in cells. (a) Co-transfection of LTR-Tax and pcDNA3-Flag-tagged Cdc37 (F-Cdc37) mutants. Lane 1: control pcDNA3 1  $\mu$ g; lane 2: LTR-Tax 0.5  $\mu$ g + pcDNA3 0.5  $\mu$ g; lane 3: LTR-Tax 0.5  $\mu$ g + F-Cdc37(1–378) wild type 0.5  $\mu$ g; lane 4: LTR-Tax 0.5  $\mu$ g + F-Cdc37(1–200) 0.5  $\mu$ g; lane 5: LTR-Tax 0.5  $\mu$ g + F-Cdc37(1–180) 0.5  $\mu$ g; lane 6: LTR-Tax 0.5  $\mu$ g + F-Cdc37(181–378) 0.5  $\mu$ g; lane 7: LTR-Tax 0.5  $\mu$ g + F-Cdc37(201–378) 0.5  $\mu$ g. After 40 h transfection, HEK293 cells were lysed with 100  $\mu$ l of lysis buffer, and the NF- $\kappa$ B-dependent luciferase activity was normalized with  $\beta$ -galactosidase value (upper panel). A portion of 10  $\mu$ g of each lysate was resolved by sodium dodecyl sulfate-polyacrylamide gel electrophoresis, and the expression of Tax (middle panel) or Flag-tagged Cdc37s (lower panel) was detected by specific monoclonal antibodies. (b) Dose-dependent degradation of Tax by F-Cdc37 mutants. Lane 1: control pcDNA3 1  $\mu$ g; lanes 2–11: 0.5  $\mu$ g of LTR-Tax; lanes 3–5: plus 0.125, 0.25 and 0.5  $\mu$ g of F-Cdc37(1–200); lanes 6–8: plus 0.125, 0.25 and 0.5  $\mu$ g of F-Cdc37(1–180); lanes 9–11: plus 0.125, 0.25 and 0.5  $\mu$ g of F-Cdc37(181–378), pcDNA3 was added to normalize the DNA amount. Tax (upper panel), Flag-tagged Cdc37s (middle panel) and tubulin (lower panel) were detected by specific monoclonal antibodies. (c) Cdc37's CBD (amino-acid residues 181–200(ref. 26)) is required for Tax interaction. A portion of 0.5  $\mu$ g of control pcDNA3 (lane 1) or LTR-Tax (lanes 2–9) was transfected (lysate-1, middle panel) and 0.5  $\mu$ g of control pcDNA3 (lanes 1 and 2), F-HSP90 (lane 3), wild-type F-Cdc37(1–378, lane 4), F-Cdc37(1–278, lane 5), F-Cdc37(1–200, lane 6), F-Cdc37(1–180, lane 7), F-Cdc37(181–378, lane 8) and F-Cdc37(201–378, lane 9) were transfected separately (lysate-2, lower panel). The expression of each protein in cell lysates was detected by specific monoclonal antibodies (middle and bottom panels). A portion of 200  $\mu$ g of each lane's cell lysates was mixed and subjected to Co-IP with 2  $\mu$ g of rabbit anti-Flag antibodies, and each Co-IP complex was washed four times with Co-IP buffer, and following sodium dodecyl sulfate-polyacrylamide gel electrophoresis, Tax was detected by anti-Tax antibody (upper panel). (d) GFP two-hybrid binding assay between Cdc37 and Tax. HEK293 cells transfected with the six-well plates were transfected with phmKGN-MC-Tax and phmKGC-MN-Cdc37 or its mutant – Cdc37(N200) and – Cdc37(N180) by FugeneHD. After 48 h incubation, the transfected HEK293 cells were treated with Hoechst 34442 (Sigma) at the final concentration of 1  $\mu$ M. Light and fluorescent (GFP and Hoechst 34442) microscopic observation and photography were performed by BZ-9000 Biorevo all-in-one fluorescence microscope (Keyence).



activated by Tax are inhibited by 17-DMAG treatment, the simplest interpretation suggests that all these effects arise from 17-DMAG-mediated destabilization of the Tax protein itself.

The client-binding domain of CDC37 plays crucial roles in Tax stabilization and Tax-mediated NF- $\kappa$ B activation

The molecular chaperone activity of HSP90 is usually exerted in cooperation with various co-chaperones. CDC37 was identified along with HSP90 as an essential component for a TNF- $\alpha$ -activated HMW-IKK complex.<sup>12</sup> As our current study shows the involvement of HSP90 in Tax-mediated HMW-IKK formation and NF- $\kappa$ B activation,<sup>11,17</sup> we generated Flag-tagged serial deletion mutants of HSP90 and CDC37 to examine their potential effects on Tax activity.

HSP90 has three distinct functional domains as described in Supplementary Figure 3.<sup>35-37</sup> We generated five deletion mutants, N, N+M, M, M+C and C, and transduced each with a Tax expression vector into HEK293 cells to determine any dominant-negative effects. Surprisingly, none of these mutants showed suppressive effects on Tax-mediated NF- $\kappa$ B activation or Tax stabilization (data not shown).

We then investigated the possible involvement of CDC37 in Tax stabilization and NF- $\kappa$ B signaling according to its functional domains (Supplementary Figure 3), namely, an HSP90-binding domain expanding through M164 to E221,<sup>38</sup> a kinase-binding domain at amino-acid residues 40-110,<sup>39</sup> a client-binding domain (CBD, amino-acid residues 181-200),<sup>26</sup> and a self-dimerization domain (amino-acid residues 240-260).<sup>39</sup> Although overexpression of full-length CDC37 slightly enhanced NF- $\kappa$ B

activation (Figure 4a upper panel, lane 3), the mutants containing CBD, CDC37(1-200) and CDC37(181-378), strongly suppressed Tax-mediated NF- $\kappa$ B activation (Figure 4a upper panel, lanes 4 and 6) and induced extensive Tax degradation (Figure 4a middle panel, lanes 4 and 6). The mutants CDC37(1-180) and CDC37(201-378) lacking CBD had little effects on either NF- $\kappa$ B activation or Tax stability (lanes 5 and 7). Tax degradation was reconfirmed by titration of these mutants (Figure 4b). Both CCD37(1-200) and CCD37(181-378) progressively promoted Tax degradation (lanes 3-5 and 9-11, respectively), but CDC37(1-180) had little effects (lanes 6-8). Coexpression of certain sets of CDC37 mutants could promote Tax degradation through impaired physical interaction with Tax. We transfected HEK293 cells with Tax or Flag-CDC37 expression vectors separately to avoid spontaneous Tax degradation, and each cell lysate was mixed and applied for Co-IP experiments with anti-Flag antibodies (Figure 4c). Each protein expression was confirmed by immunoblotting for Tax (middle panel) or Flag (lower panel). Although the immunoprecipitates from wild-type HSP90 (upper panel, lane 3), CDC37 (lane 4) and Tax-degrading CDC37(1-200) and CDC37(181-378) (lanes 6 and 8) contained Tax in the complex, the immunoprecipitates from CDC37(1-180) and CDC37(201-378) lacking Tax-degrading properties did not (lanes 7 and 9).

Finally, we examined direct interaction between the two proteins using a GFP two-hybrid assay. Tax, tagged with the N-terminal portion of Kusabira-Green<sup>27</sup> fluorescent protein, and CDC37s (1-378, 1-200 and 1-180), tagged with the C-terminal portion, were co-transfected into HEK293 cells. Consistent with Co-IP results, co-transfectants of Tax and CDC37(1-378) or CDC37(1-200) emitted green fluorescence but Tax plus CDC37

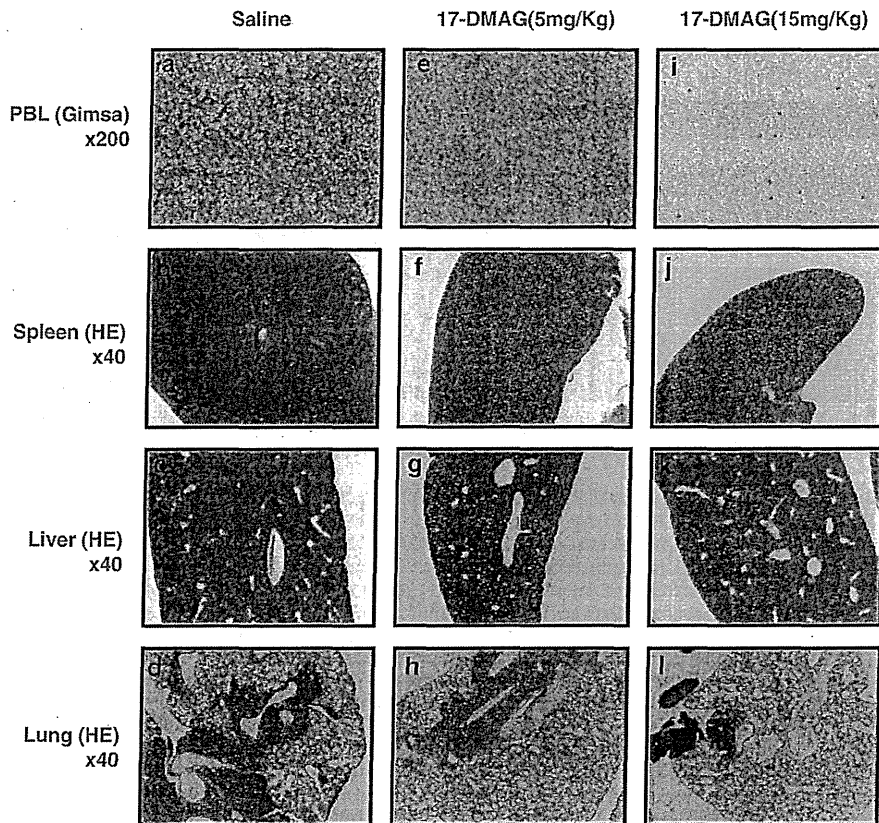


**Figure 5.** Oral administration of 17-DMAG blocks aggressive infiltration of Lck-Tax Tg cells into multiple organs of SCID mice. Two million Lck-Tax Tg cells were injected intraperitoneally into SCID mice. 17-DMAG was administered orally 5 days per week, with 5 mg/kg body weight (e-h) or 15 mg/kg body weight (i-l) or untreated (a-d). Mice were sacrificed after 21 days incubation, and organs were processed for Giemsa (a, e, i) or hematoxylin and eosin (HE, b-d, f-h and j-l) staining. Microscopic observations were performed and photographed with indicated magnifications. Tg, transgenic.

(1–180) did not. The Tax–CDC37(1–200) complex was translocated to the nucleus, whereas Tax–CDC37(1–378; wild type) stayed in the cytoplasm (Figure 4d). Collectively, these findings suggested the direct involvement of CDC37 for Tax stabilization.

An oral administration of 17-DMAG to ATL model mice induced blockade of aggressive proliferation and multiple tissue invasions of transformed lymphocytes and improved survival rate

The demonstration that 17-DMAG has profound effects on Tax stability and the fact that it is water soluble suggested that this compound could be tested in a recently developed preclinical model of ATL.<sup>23,28</sup>

SCID mice were injected with  $2 \times 10^6$  Lck-Tax cells intraperitoneally and treated for 5 consecutive days per week for 2 weeks with saline alone or with 17-DMAG in saline at 5 or 15 mg/kg. Mice were euthanized 21 days after cell inoculation. The blood smear indicated apparent reduction of Lck-Tax cells with increasing doses of 17-DMAG to saline controls (Figures 5a, e and i), although the quantitative cell counts were not obtained. The white pulp in greatly enlarged spleens (splenomegaly) of control mice was markedly expanded with red pulp compression (Figure 5b), and the livers and lungs of saline control mice were characterized by extensive perivascular infiltrations with Lck-Tax cells (Figures 5c and d). These pathologies were progressively reduced in mice treated with 17-DMAG (spleen, Figures 5f and j; liver, Figures 5g and k; and lung, Figures 5h and l).

We then determined the survival improvement through 17-DMAG oral administration with another preclinical ATL model (Figure 6). Each 7 (14 in total) huNOG mice<sup>28</sup> were injected with  $1 \times 10^6$  HTLV-1-producing JEX cells (details are described in Supplementary Information), and 2 weeks after inoculation, each 4 of these mice (8 in total) were treated 20 times with 15 or 25 mg/kg of 17-DMAG for 4 weeks (as shown in Supplementary Figure 4), whereas the remaining 6 mice received saline only. The percentage of CD25-positive T cells, proviral load and the number of human leukocytes in peripheral blood were monitored. Four of eight 17-DMAG-treated mice died within 8 weeks post inoculation probably because of high drug dosage, but other four mice (50%) survived more than 20 weeks, whereas all the saline-treated controls died within 12 weeks post inoculation. The average survival period of controls and 17-DMAG-treated subjects were 8.33 and 14.75 weeks, respectively. However, the survival periods of 17-DMAG-treated subjects could be extended because four subjects were sacrificed at 24 weeks post inoculation for pathological examination (Supplementary Figure 4). The numbers of HTLV-1-infected human leukocytes in peripheral blood of 17-DMAG-treated subjects were also 5–10 times fewer than those of saline controls (Figures 6b and c).

Additive effects for growth arrest and apoptosis induction by concomitant 17-DMAG/Nutlin-3a treatment against ATL cells

The standard chemotherapy against ATL, named as leukemia study group 15 (LSG15), is currently employing the combination of four different anticancer drugs that frequently brings serious side effects to patients.<sup>40</sup> We previously demonstrated that a novel MDM-2-antagonizing/p53-stabilizing drug, Nutlin-3a, induces

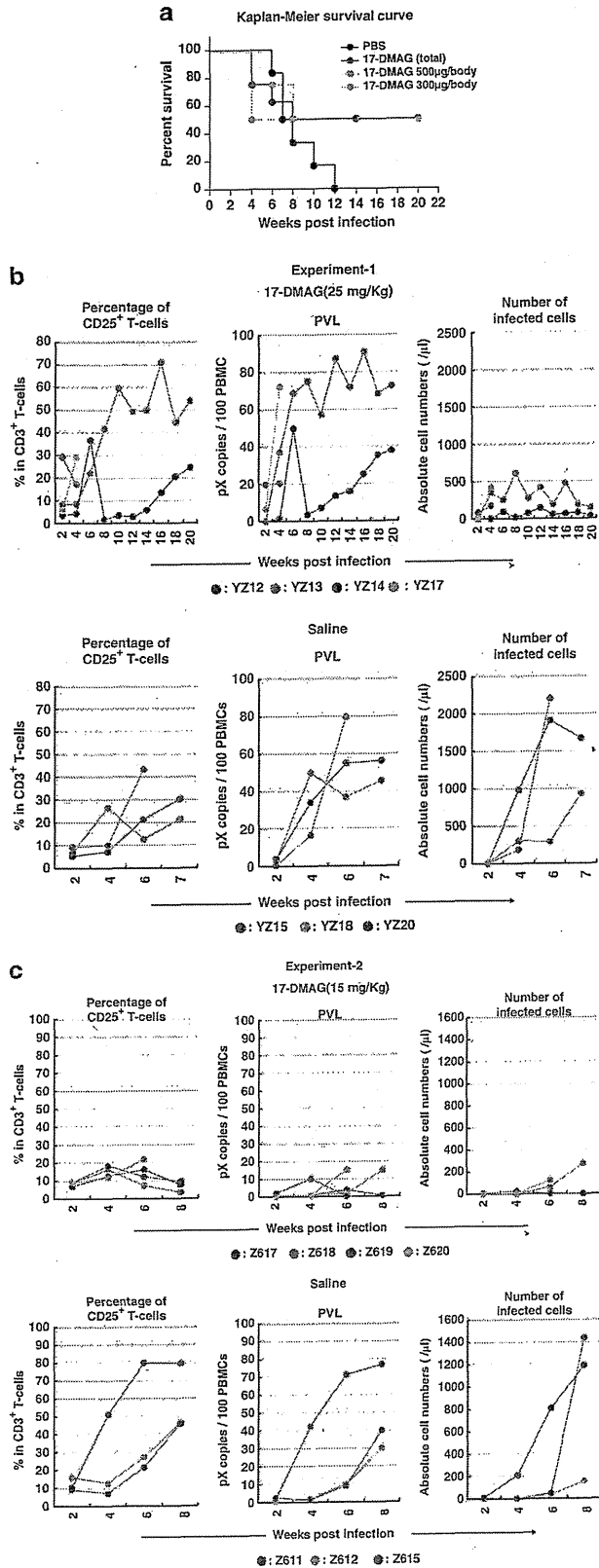


**Figure 6.** Improved survival and suppression of the growth of HTLV-1-infected T cells by 17-DMAG oral treatment. (a) Kaplan-Meier survival curve of HTLV-1-infected huNOG mice. All mice have reconstituted human immune system by the transplantation of hematopoietic stem cells (huNOG) and have received 1 million JEX cells, which produce HTLV-1 infectious virus (see the details in Supplementary Figure 4). JEX/huNOG mice received 17-DMAG by oral administration for 4 weeks (2–6 weeks post inoculation, five times/week) at the dosage of 25 mg/kg (orange line) and 15 mg/kg (pink line). Control mice received the same volume of PBS. (b) The percentage of CD25-positive T cells, PVL and the number of HTLV-1-infected cells in peripheral blood of infected mice are shown. Upper panel represents the results from 17-DMAG-treated (25 mg/kg) mice; lower panel represents those of control mice. (c) Same experiments with 17-DMAG (15 mg/kg, upper panel) and PBS control (lower panel). PBS, phosphate buffered saline; PVL, proviral load.



the senescent death to ATL cells.<sup>41</sup> We then examined the additive anti-ATL effects of 17-DMAG and Nutlin-3a. Suboptimal dose of 17-DMAG (0.1  $\mu\text{M}$ ) or Nutlin-3a (1  $\mu\text{M}$ ) alone did not induce sufficient apoptotic or growth-arrest activities to ATL cell lines. However, the combined use of both induced significant growth suppressive and apoptotic properties (Figure 7), suggesting the possible combinational use of these drugs for further clinical studies.

**DISCUSSION**

HTLV-1 is the etiologic agent of ATL. Current studies indicate that worldwide there are more than 20 million HTLV-1 carriers and that 5% of these carriers will develop ATL.<sup>42</sup> The current standard for treatment of acute- or lymphoma-type ATL in Japan is CHOP or its modified regimen LSG15; however, the responses to this treatment regimen are limited to 31.1% of patients with 2-year survivals.<sup>40</sup> As malignant cells from relapsed patients are also resistant to other chemotherapeutic interventions, novel strategies for treatment of ATL are urgently required.

In this study, we demonstrated the significant inhibitory effects of 17-DMAG on Tax-mediated NF- $\kappa\text{B}$  signaling *in vitro* and *ex vivo*. The most striking observations obtained *in vitro* were (a) 17-DMAG-induced Tax degradation that resulted from inhibiting the formation of the Tax-IKK-HSP90/CDC37 ternary complex (Figures 1a-d); (b) induction of growth suppression and apoptosis of ATL cells while having little or no effect on normal PBLs (Figures 2a and b). We also found that the stability of Tax was heavily dependent on the CBD of CDC37 (Figures 4a and b).

GA-dependent NF- $\kappa\text{B}$  downregulation in ATL cells was reported, and inhibition of autophagic activity seemed to affect the conversion of p100 (NF- $\kappa\text{B}$ 2 precursor) to active p52.<sup>32</sup> We observed this time 17-DMAG-dependent Tax degradation and its blockade by AICAR and 3-MA (autophagy inhibitors) but not by the proteasome inhibitor MG-132 (Figure 1d), suggesting the direct involvement of the autophagosome on Tax metabolism in cells. This issue should further be investigated with ubiquitylation-deficient mutants Tax<sup>24,31</sup> or the autophagy-deficient cells.<sup>43,44</sup>

The CBD of CDC37 has been reported to bind preferentially to a specific glycine-rich motif — GXGXGXG.<sup>45</sup> Indeed, Tax has a similar motif in its N terminus. CBD played crucial roles in stabilizing Tax and Tax-CDC37 complex formation (Figures 4c and d). CBD-containing mutants of CDC37 seemed to enhance the machinery responsible for Tax degradation as we did not detect any decrease in Tax levels in response to an siRNA knockdown of CDC37 (Supplementary Figure 5). Interestingly, the Tax-destabilizing CDC37(N200) translocated Tax to the nucleus, whereas wild-type CDC37 stayed with Tax in the cytoplasm (Figure 4d), and it implies that this translocation could be related to the Tax destabilization. For the future, it would be worth trying to identify a chemical compound that mimics the structure of CBD and could function as an inducer of Tax degradation. HSP90 and its co-chaperone's involvement in multiple signaling cascades, especially, in cancer cells, has been reported.<sup>46,47</sup> Indeed, 17-DMAG also suppressed NF- $\kappa\text{B}$  signaling mediated by other activators NIK, MEKK1, AKT, TAB2 and IKK $\alpha/\beta$  (data not shown). We also found that 17-DMAG treatment induced Tax degradation; potentially 17-DMAG treatment may also have led to the destabilization of other NF- $\kappa\text{B}$  signaling activators.

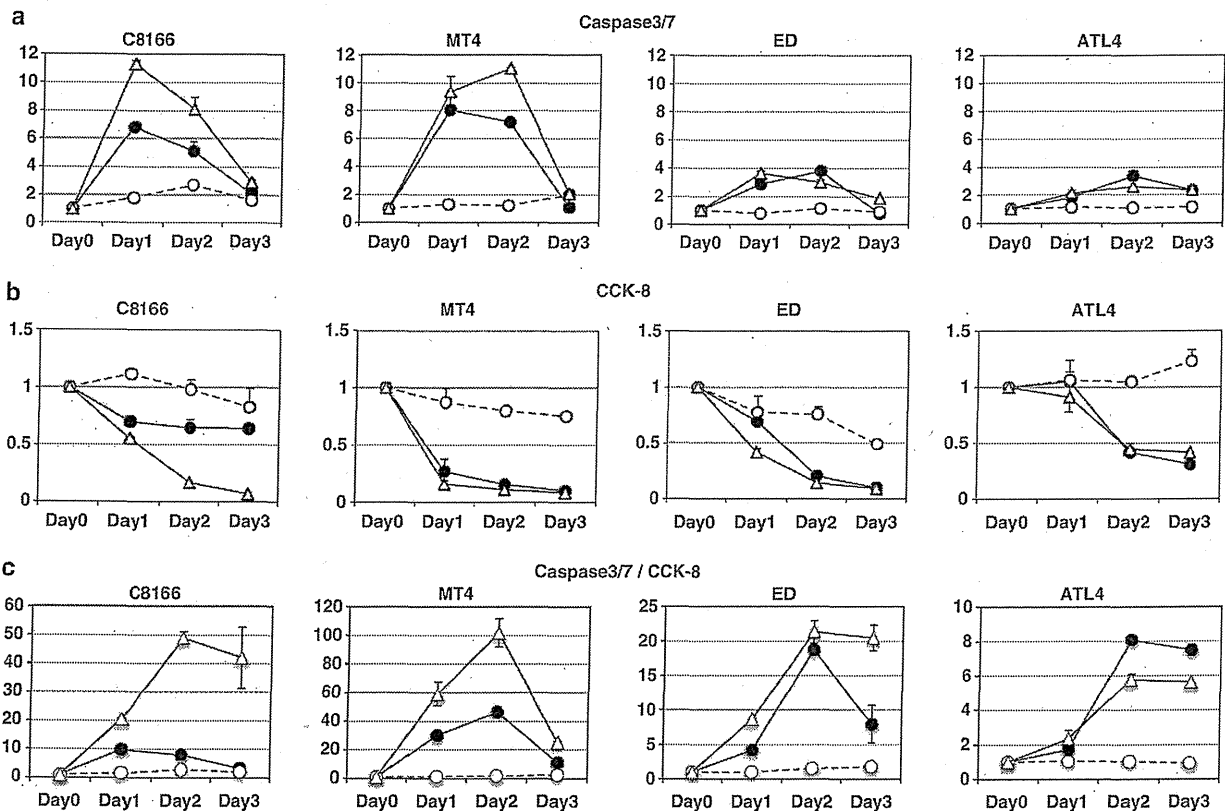


**Figure 7.** Additive anti-ATL cell effects by the combined dosage of 17-DMAG and Nutlin-3a. (a) ATL cell lines C8166, MT4, ED and ATL4 were treated with either suboptimal single dose of 17-DMAG (0.1  $\mu\text{M}$ , black circles) and Nutlin-3a (1  $\mu\text{M}$ , white circles)<sup>41</sup> or both (white triangles) for 3 days and harvested for caspase-3/7 assays (a) or CCK-8 assays (b) as described in Figure 2. Each untreated cell's value was set as 1. (c) Each caspase-3/7 (apoptotic) value was divided by CCK-8 (growth arrest) value to manifest the additive effects (see the Discussion section). CCK-8, Cell Counting Kit 8.

We have determined the therapeutic effects of 17-DMAG on two different ATL model systems through its oral administration. First, we tested 17-DMAG induced prevention of Lck-Tax infiltration in SCID mice, and 5 and 15 mg/kg of oral administration of 17-DMAG for 2 weeks reduced 74% and 83% of Lck-Tax cells, respectively; splenomegaly or massive infiltration of Lck-Tax cells into livers and lungs was also significantly reduced (Figure 5). In all experiments, 17-DMAG mice did not show any body weight losses or inactiveness compared with saline controls.

We then switched to another ATL model experiment JEX/huNOG, which has humanized immune environment in NOG mice and has inoculated HTLV-1-producing Jurkat cells. With oral administration of both 15 and 25 mg/kg 17-DMAG to JEX/huNOG, four of eight mice survived more than 20 weeks, whereas saline controls died within 12 weeks (Figure 6a). 17-DMAG treatment also reduced the number of HTLV-1-infected cells in peripheral blood, suggesting that 17-DMAG treatment could intervene the clonal T-cell development to ATL (Figure 6b). Although this preliminary experiment did not provide statistically significant survival rates, efficacy of this treatment is indeed highly expected. It is necessary to find the optimized conditions suppressing the ATL cell proliferation without any serious side effects.

Tax has pleiotropic effects on intra-cellular or inter-cellular signalings including mitotic checkpoint disruption,<sup>48</sup> aberrant cell-cycle progression<sup>49,50</sup> and altered chemotaxis.<sup>51</sup> The present ATL treatment protocols target the cytoskeletons or DNA replications with multiple doses of anticancer drugs (called as LSG15), and significant side effects by this treatment have been frequently recognized.<sup>40</sup> We have recently demonstrated the potential uses of molecularly targeted inhibitors of ATL cell proliferation, such as a MDM-2 ubiquitin ligase inhibitor Nutlin-3a<sup>41</sup> or CXCR4 antagonist AMD3100.<sup>51</sup> Nutlin-3a induces growth arrest and senescent-cell death of ATL cells at the 10  $\mu$ M concentration, but normal PBLs are also significantly affected.<sup>41</sup> The combined use of 17-DMAG (0.1  $\mu$ M) and Nutlin-3a (1  $\mu$ M), suboptimal concentration for single use, significantly enhanced both apoptotic and growth suppressive effects (Figures 7a and b). This concurrent effects can be manifested with the division of caspase-3/7 values by Cell Counting Kit 8 values (Figure 7c). Besides Nutlin-3a, we also tested the efficacy of 17-DMAG plus LSG15 (without prednisolone; Supplementary Figure 6). Unlike the results of 17-DMAG/Nutlin-3a, 17-DMAG/LSG15 did not show any clear additive effects probably because LSG15 affects cell-cycle progression with a wide range of spectrum, but the effects of Nutlin-3a are specifically restricted to p53 stabilization.

It remains to be seen whether 17-DMAG is effective for ATL patients' treatment; elsewhere Hertlein *et al.*<sup>52</sup> have reported 17-DMAG's clinical application against chronic lymphocytic leukemia. Perhaps in future studies, 17-DMAG and other new drugs with novel anti-ATL activities such as Nutlin-3a, AMD3100 or a monoclonal anti-CCR4 antibody (KW-0761)<sup>53</sup> will provide more effective and less toxic ATL therapy.

#### CONFLICT OF INTEREST

The authors declare no conflict of interest.

#### ACKNOWLEDGEMENTS

We are indebted to Dr Herbert C Morse III for his helpful discussion and comments. We thank Mr T Kawashima and Ms Y Itoh for technical assistance and Drs K Terasawa, C Pique and K Nagata for providing plasmid DNAs. EI was a research fellow of the Okinawa Science and Technology Promotion Center. This study was supported in part by grants from the Ministry of Education, Culture, Sports, Science and Technology; the Ministry of Health, Labor and Welfare; the Ministry of Economy, Trade and Industry; Japan Science and Technology Agency; Okinawa Science and Technology Promotion Center; and Miyazaki Prefectural Industrial Support Foundation.

#### AUTHOR CONTRIBUTIONS

HI, J-IF and HdH designed the research; HdH, HS, WWH, KT, TU and J-IF developed the ATL animal model; EI, AK, KT, ST, SH, TMa, TU, TMI, KS, J-IF, HdH and HI performed the research; AN, MH, HrH, YY, YT, HS, WH, YM, KTJ, MO and KM contributed new reagents/materials; AK, KT, J-IF and HdH contributed pathologic analysis; and EI, KT, J-IF, HdH and HI wrote the paper.

#### REFERENCES

- Li Q, Verma IM. NF-kappaB regulation in the immune system. *Nat Rev Immunol* 2002; **2**: 725-734.
- Janssens S, Tschopp J. Signals from within: the DNA-damage-induced NF-kappaB response. *Cell Death Differ* 2006; **13**: 773-784.
- Karin M. NF-kappaB as a critical link between inflammation and cancer. *Cold Spring Harb Perspect Biol* 2009; **1**: a000141.
- Hayden MS, Ghosh S. Shared principles in NF-kappaB signaling. *Cell* 2008; **132**: 344-362.
- Li XH, Fang X, Gaynor RB. Role of IKK-gamma/NEMO in assembly of the I-kappaB kinase complex. *J Biol Chem* 2001; **276**: 4494-4500.
- Li Q, Van Antwerp D, Mercurio F, Lee KF, Verma IM. Severe liver degeneration in mice lacking the I-kappaB kinase 2 gene. *Science* 1999; **284**: 321-325.
- Schmidt-Supprian M, Bloch W, Courtois G, Adicks K, Israel A, Rajewsky K *et al.* NEMO/IKK-gamma-deficient mice model incontinentia pigmenti. *Mol Cell* 2000; **5**: 981-992.
- Li Q, Lu Q, Hwang JY, Buscher D, Lee KF, Izpisua-Belmonte JC *et al.* IKK1-deficient mice exhibit abnormal development of skin and skeleton. *Genes Dev* 1999; **13**: 1322-1328.
- Takeda K, Takeuchi O, Tsujimura T, Itami S, Adachi O, Kawai T *et al.* Limb and skin abnormalities in mice lacking IKK-alpha. *Science* 1999; **284**: 313-316.
- Yamaoka S, Courtois G, Bessia C, Whiteside ST, Weil R, Agou F *et al.* Complementation cloning of NEMO, a component of the I-kappaB kinase complex essential for NF-kappaB activation. *Cell* 1998; **93**: 1231-1240.
- Iha H, Kibler KV, Yedavalli VR, Peloponese JM, Haller K, Miyazato A *et al.* Segregation of NF-kappaB activation through NEMO/IKK-gamma by Tax and TNF-alpha: implications for stimulus-specific interruption of oncogenic signaling. *Oncogene* 2003; **22**: 8912-8923.
- Chen G, Cao P, Goeddel DV. TNF-induced recruitment and activation of the IKK complex require Cdc37 and Hsp90. *Mol Cell* 2002; **9**: 401-410.
- Bouwmeester T, Bauch A, Ruffner H, Angrand PO, Bergamini G, Croughton K *et al.* A physical and functional map of the human TNF-alpha/NF-kappa B signal transduction pathway. *Nat Cell Biol* 2004; **6**: 97-105.
- Yoshida M. Multiple viral strategies of HTLV-1 for dysregulation of cell growth control. *Annu Rev Immunol* 2001; **19**: 475-496.
- Hall WW, Fujii M. Deregulation of cell-signaling pathways in HTLV-1 infection. *Oncogene* 2005; **24**: 5965-5975.
- Matsuoka M, Jeang KT. Human T-cell leukaemia virus type 1 (HTLV-1) infectivity and cellular transformation. *Nat Rev Cancer* 2007; **7**: 270-280.
- Jin DY, Giordano V, Kibler KV, Nakano H, Jeang KT. Role of adapter function in oncoprotein-mediated activation of NF-kappaB. Human T-cell leukemia virus type 1 Tax interacts directly with I-kappaB kinase gamma. *J Biol Chem* 1999; **274**: 17402-17405.
- Carter RS, Pennington KN, Ungurait BJ, Ballard DW. *In vivo* identification of inducible phosphoacceptors in the IKK-gamma/NEMO subunit of human I-kappaB kinase. *J Biol Chem* 2003; **278**: 19642-19648.
- Lamsoul I, Lodewick J, Lebrun S, Brasseur R, Burny A, Gaynor RB *et al.* Exclusive ubiquitination and sumoylation on overlapping lysine residues mediate NF-kappaB activation by the human T-cell leukemia virus Tax oncoprotein. *Mol Cell Biol* 2005; **25**: 10391-10406.
- Chu ZL, DiDonato JA, Hawiger J, Ballard DW. The Tax oncoprotein of human T-cell leukemia virus type 1 associates with and persistently activates I-kappaB kinases containing IKK-alpha and IKK-beta. *J Biol Chem* 1998; **273**: 15891-15894.
- Geleziunas R, Ferrell S, Lin X, Mu Y, Cunningham Jr ET, Grant M *et al.* Human T-cell leukemia virus type 1 Tax induction of NF-kappaB involves activation of the I-kappaB kinase alpha (IKK-alpha) and IKK-beta cellular kinases. *Mol Cell Biol* 1998; **18**: 5157-5165.
- Egorin MJ, Lagattuta TF, Hamburger DR, Covey JM, White KD, Musser SM *et al.* Pharmacokinetics, tissue distribution, and metabolism of 17-(dimethylaminoethylamino)-17-demethoxygeldanamycin (NSC 707545) in CD2F1 mice and Fischer 344 rats. *Cancer Chemother Pharmacol* 2002; **49**: 7-19.
- Hasegawa H, Sawa H, Lewis MJ, Orba Y, Sheehy N, Yamamoto Y *et al.* Thymus-derived leukemia-lymphoma in mice transgenic for the Tax gene of human T-lymphotropic virus type I. *Nat Med* 2006; **12**: 466-472.

- 24 Chiari E, Lamsoul I, Lodewick J, Chopin C, Bex F, Pique C. Stable ubiquitination of human T-cell leukemia virus type 1 tax is required for proteasome binding. *J Virol* 2004; **78**: 11823–11832.
- 25 Momose F, Naito T, Yano K, Sugimoto S, Morikawa Y, Nagata K. Identification of Hsp90 as a stimulatory host factor involved in influenza virus RNA synthesis. *J Biol Chem* 2002; **277**: 45306–45314.
- 26 Terasawa K, Minami Y. A client-binding site of Cdc37. *FEBS J* 2005; **272**: 4684–4690.
- 27 Ueyama T, Kusakabe T, Karasawa S, Kawasaki T, Shimizu A, Son J *et al*. Sequential binding of cytosolic Phox complex to phagosomes through regulated adaptor proteins: evaluation using the novel monomeric Kusabira-Green system and live imaging of phagocytosis. *J Immunol* 2008; **181**: 629–640.
- 28 Nie C, Sato K, Misawa N, Kitayama H, Fujino H, Hiramatsu H *et al*. Selective infection of CD4+ effector memory T lymphocytes leads to preferential depletion of memory T lymphocytes in R5 HIV-1-infected humanized NOD/SCID/IL-2Rgmanull mice. *Virology* 2009; **394**: 64–72.
- 29 Ueno S, Umeki K, Takajo I, Nagatomo Y, Kusumoto N, Umekita K *et al*. Proviral loads of human T-lymphotropic virus type 1 in asymptomatic carriers with different infection routes. *Int J Cancer* 2012; **130**: 2318–2326.
- 30 De Valck D, Jin DY, Heynink K, Van de Craen M, Contreras R, Fiers W *et al*. The zinc finger protein A20 interacts with a novel anti-apoptotic protein which is cleaved by specific caspases. *Oncogene* 1999; **18**: 4182–4190.
- 31 Peloponese JM, Iha H, Yedavalli VR, Miyazato A, Li Y, Haller K *et al*. Ubiquitination of human T-cell leukemia virus type 1 tax modulates its activity. *J Virol* 2005; **78**: 11686–11695.
- 32 Yan P, Qing G, Qu Z, Wu CC, Rabson A, Xiao G. Targeting autophagic regulation of NFkappaB in HTLV-1 transformed cells by geldanamycin: implications for therapeutic interventions. *Autophagy* 2007; **3**: 600–603.
- 33 Mitsiades CS, Mitsiades NS, McMullan CJ, Poulaki V, Kung AL, Davies FE *et al*. Antimyeloma activity of heat shock protein-90 inhibition. *Blood* 2006; **107**: 1092–1100.
- 34 Jeang KT, Chiu R, Santos E, Kim SJ. Induction of the HTLV-1 LTR by Jun occurs through the Tax-responsive 21-bp elements. *Virology* 1991; **181**: 218–227.
- 35 Prodromou C, Roe SM, O'Brien R, Ladbury JE, Piper PW, Pearl LH. Identification and structural characterization of the ATP/ADP-binding site in the Hsp90 molecular chaperone. *Cell* 1997; **90**: 65–75.
- 36 Meyer P, Prodromou C, Hu B, Vaughan C, Roe SM, Panaretou B *et al*. Structural and functional analysis of the middle segment of hsp90: implications for ATP hydrolysis and client protein and cochaperone interactions. *Mol Cell* 2003; **11**: 647–658.
- 37 Minami Y, Kimura Y, Kawasaki H, Suzuki K, Yahara I. The carboxy-terminal region of mammalian HSP90 is required for its dimerization and function *in vivo*. *Mol Cell Biol* 1994; **14**: 1459–1464.
- 38 Roe SM, Ali MM, Meyer P, Vaughan CK, Panaretou B, Piper PW *et al*. The mechanism of Hsp90 regulation by the protein kinase-specific cochaperone p50(cdc37). *Cell* 2004; **116**: 87–98.
- 39 Silverstein AM, Grammatikakis N, Cochran BH, Chinkers M, Pratt WB. p50(cdc37) binds directly to the catalytic domain of Raf as well as to a site on hsp90 that is topologically adjacent to the tetratricopeptide repeat binding site. *J Biol Chem* 1998; **273**: 20090–20095.
- 40 Uozumi K. Treatment of adult T-cell leukemia. *J Clin Exp Hematop* 2010; **50**: 9–25.
- 41 Hasegawa H, Yamada Y, Iha H, Tsukasaki K, Nagai K, Atogami S *et al*. Activation of p53 by Nutlin-3a, an antagonist of MDM2, induces apoptosis and cellular senescence in adult T-cell leukemia cells. *Leukemia* 2009; **23**: 2090–2101.
- 42 Proietti FA, Carneiro-Proietti AB, Catalan-Soares BC, Murphy EL. Global epidemiology of HTLV-1 infection and associated diseases. *Oncogene* 2005; **24**: 6058–6068.
- 43 Mizushima N, Yoshimori T, Ohsumi Y. The role of Atg proteins in autophagosome formation. *Annu Rev Cell Dev Biol* 2011; **27**: 107–132.
- 44 Codogno P, Mehrpour M, Proikas-Cezanne T. Canonical and non-canonical autophagy: variations on a common theme of self-eating? *Nat Rev Mol Cell Biol* 2011; **13**: 7–12.
- 45 Terasawa K, Yoshimatsu K, Iemura SI, Natsume T, Tanaka K, Minami Y. Cdc37 interacts with the glycine-rich loop of Hsp90 client kinases. *Mol Cell Biol* 2006; **26**: 3378–3389.
- 46 Calderwood SK, Khaleque MA, Sawyer DB, Ciocca DR. Heat shock proteins in cancer: chaperones of tumorigenesis. *Trends Biochem Sci* 2006; **31**: 164–172.
- 47 Caplan AJ, Mandal AK, Theodoraki MA. Molecular chaperones and protein kinase quality control. *Trends Cell Biol* 2007; **17**: 87–92.
- 48 Jin DY, Spencer F, Jeang KT. Human T cell leukemia virus type 1 oncoprotein Tax targets the human mitotic checkpoint protein MAD1. *Cell* 1998; **93**: 81–91.
- 49 Giam CZ, Jeang KT. HTLV-1 Tax and adult T-cell leukemia. *Front Biosci* 2007; **12**: 1496–1507.
- 50 Tanaka Y. Activation of leukocyte function-associated antigen-1 on adult T-cell leukemia cells. *Leuk Lymphoma* 1999; **36**: 15–23.
- 51 Kawaguchi A, Orba Y, Kimura T, Iha H, Ogata M, Tsuji T *et al*. Inhibition of the SDF-1alpha-CXCR4 axis by the CXCR4 antagonist AMD3100 suppresses the migration of cultured cells from ATL patients and murine lymphoblastoid cells from HTLV-1 Tax transgenic mice. *Blood* 2009; **114**: 2961–2968.
- 52 Hertlein E, Wagner AJ, Jones J, Lin TS, Maddocks KJ, Towns III WH *et al*. 17-DMAG targets the nuclear factor-kappaB family of proteins to induce apoptosis in chronic lymphocytic leukemia: clinical implications of HSP90 inhibition. *Blood* 2010; **116**: 45–53.
- 53 Yamamoto K, Utsunomiya A, Tobinai K, Tsukasaki K, Uike N, Uozumi K *et al*. Phase I study of KW-0761, a defucosylated humanized anti-CCR4 antibody, in relapsed patients with adult T-cell leukemia-lymphoma and peripheral T-cell lymphoma. *J Clin Oncol* 2010; **28**: 1591–1598.



This work is licensed under a Creative Commons Attribution-NonCommercial-NoDerivs 3.0 Unported License. To view a copy of this license, visit <http://creativecommons.org/licenses/by-nc-nd/3.0/>

Supplementary Information accompanies this paper on the Blood Cancer Journal website (<http://www.nature.com/bcj>).

## Increased Plasma Caveolin-1 Levels Are Associated with Progression of Prostate Cancer among Japanese Men

SATORU SUGIE<sup>1</sup>, SHOICHIRO MUKAI<sup>1</sup>, HIROMASA TSUKINO<sup>1</sup>, YOSHINOBU TODA<sup>3</sup>,  
TAKENORI YAMAUCHI<sup>2</sup>, ICHIRO NISHIKATA<sup>4</sup>, YOSHIKI KURODA<sup>2</sup>,  
KAZUHIRO MORISHITA<sup>4</sup> and TOSHIYUKI KAMOTO<sup>1</sup>

Departments of <sup>1</sup>Urology, <sup>2</sup>Public Health, and <sup>4</sup>Tumor and Cellular Biochemistry,  
Faculty of Medicine, University of Miyazaki, Miyazaki, Japan;

<sup>3</sup>Laboratory Medicine, Faculty of Health Care, Tenri Health Care University, Tenri, Japan

**Abstract.** *Aim: Up-regulation of caveolin-1 (CAVI) is associated with aggressive prostate cancer. Among Caucasian and African-American patients, plasma CAVI levels are elevated in patients with castration-resistant prostate cancer (CRPC), but not in those with hormone-sensitive prostate cancer (non-CRPC), which implies that CAVI could be a therapeutic target for CRPC. Here, we evaluated associations between plasma CAVI levels and these types of cancer in Japanese men, and CAVI expression in PC3 (CRPC) and LNCaP (non-CRPC) cell lines. Materials and Methods: Plasma samples were obtained from 58 patients with prostate cancer: 36 with CRPC and 22 with non-CRPC. Enzyme-linked immuno sorbent assay (ELISA) kits were used to determine CAVI plasma levels; qRT-PCR and western blots were used to evaluate the expression of CAVI mRNA and protein in cell lines. Results: Plasma CAVI levels in patients with CRPC were greatly higher than in those with non-CRPC (1.46±1.37 ng/ml in CRPC; 0.56±0.32 ng/ml in non-CRPC,  $p<0.004$ ). Western blot and real-time qRT-PCR showed CAVI protein and mRNA in PC3 cells to be significantly overexpressed compared to its expression in LNCaP cells ( $p<0.0001$ ). Conclusion: Our results showed a relationship between CAVI expression and prostate cancer progression, and support the possibility of CAVI as a therapeutic target for CRPC.*

Prostate cancer is the sixth leading cause of cancer-related death among Japanese men (1). In most cases, death from prostate cancer results from metastatic disease. Understanding the mechanisms underlying the progression of prostate cancer

will facilitate the development of biomarkers and novel therapeutic strategies to control this devastating malignancy. Caveolin-1, encoded by *CAVI*, is a major structural component of the caveolae, which are specialized plasma membrane invaginations involved in multiple cellular processes such as molecular transport, cell adhesion and signal transduction (2). Although *CAVI* may suppress tumorigenesis under some conditions (3), it is associated with, and contributes to, malignant progression through various mechanisms (4, 5).

The role of *CAVI* in cancer cells remains controversial. It is down-regulated in tumors such as human ovarian carcinoma (6) and head and neck squamous cell carcinoma (SCC) (7), which implies a tumor-suppressor role. However, *CAVI* overexpression is associated with more aggressive behavior, increased recurrence and poorer prognosis in prostate cancer in Caucasian patients (8) and in hepatocellular carcinoma (9). As these discrepancies show, whether *CAVI* up- or down-regulation is an optimistic sign in tumorigenesis, is unclear.

Emerging evidence of a role for *CAVI* in prostate cancer prompted us to investigate its activity in different prostate cancer types, such as castration-resistant prostate cancer (CRPC) and hormone-sensitive prostate cancer. We, therefore, aimed to determine the plasma *CAVI* levels and their association with prostate cancer progression. We also analyzed *CAVI* expression in the PC3 (CRPC model) and LNCaP (non-CRPC model) cell lines. To the best of our knowledge, this is the first study to evaluate the contribution of plasma *CAVI* levels to different types of prostate cancer among Japanese patients.

### Materials and Methods

**Study participants.** The study population consisted of 58 Japanese men with prostate cancer, including 36 with CRPC and 22 with non-CRPC, such as organ-confined tumors. These patients were treated at the Department of Urology, in the Miyazaki Medical University Hospital and its related hospitals between August 2011 and October

**Correspondence to:** Hiromasa Tsukino, Department of Urology, Faculty of Medicine, University of Miyazaki, 5200 Kihara, Kiyotake-cho, Miyazaki 889-1692, Japan. Tel: +81 985852968, Fax: +81 985856958, e-mail: htsukino@fc.miyazaki-u.ac.jp

**Key Words:** Caveolin-1, prostate cancer, ELISA, progression.

2012. Tumor grade was evaluated in these samples using the Gleason scoring system. All participants were informed of the details, procedures and objectives of this study. This study was approved by the Ethics Committee of Miyazaki Medical University and related hospitals (Approved number 847, August 2011).

**Enzyme-Linked Immuno Sorbent Assay (ELISA) protocols.** Blood (5 ml in EDTA<sub>2</sub>Na) were collected by venipuncture and immediately after blood sampling, plasma was obtained by centrifugation at 12,000 rcf xg for 15 min at 4°C and stored at -80°C until later analysis. To determine plasma CAVI levels, the Human Caveolin-1 ELISA Kit (Uscn Life Science, Inc., Wuhan, China; detection range=0.24-15 ng/ml) was used according to the manufacturer's instructions. To detect the concentration of plasma CAVI levels using this ELISA kit, the 60 ng/ml CAVI standard was diluted to a concentration range of 0.24-16 ng/ml in duplicate experiments and the absorption was measured

**Cell cultures.** The androgen-dependent LNCaP and androgen-independent PC3 cancer cell lines (ATCC, Manassas, VA, USA) were grown in Dulbecco's modified Eagle's medium (DMEM; Gibco, Carlsbad, CA, USA) supplemented with 10% fetal bovine serum (FBS; Gibco). Cells were grown in 9.6-cm<sup>2</sup> cell culture dishes at 37°C in a humidified atmosphere of 5% CO<sub>2</sub>. Cells were grown to 80% confluence and harvested between passages four and six by trypsinization for analysis. For western blots, cells were seeded in 9.6 cm<sup>2</sup> dishes into 2.5 ml of culture medium for LNCaP cells and PC3 cells respectively. Media were changed every day for five days; cells grown to 90% confluence were passaged by trypsinization. After centrifugation, the cell pellet was resuspended in 1 ml of protease inhibitor, and the cells were counted on a hemocytometer. Aliquots containing 50x10<sup>3</sup> cells in protease inhibitor were frozen at -80°C until used.

**Western blot analysis.** To analyze protein expression, a western blot method was used. Briefly, samples of protein of 50x10<sup>3</sup> cells were separated on a 12% polyacrylamide gel and the proteins transferred to a polyvinylidene fluoride (PVDF) membrane (transblot transfer medium; BioRad, Hercules, CA, USA). The membrane was probed with rabbit anti-cav1 (Cell Signaling Co., Boston, MA, USA), 1:1,000 diluted in Phosphate Buffered Saline (PBS) with 0.02% (v/v) Tween-20 and 3% (w/v) milk powder. Membranes were incubated with horseradish peroxidase-conjugated goat anti-rabbit immunoglobulins (Dako, Glostrup, Denmark), before detection of antibody binding by chemiluminescence (GE, Tokyo, Japan). Band intensity was measured using a LAS3000 (FUJIFILM, Tokyo, Japan) imaging densitometer and quantified by densitometry using the Image J software (National Institutes of Health, Bethesda, MD, USA).

**Real time qRT-PCR.** Total RNA was extracted from cells using the RNA Mini kit (Ambion, Paisley, OR, USA) according to the manufacturer's instructions. Genes of interest were amplified from 2 mg DNase I-treated total RNAs using Thunderbird Reverse Transcriptase (ToYoBo, Tokyo, Japan) and random primer. The primers used for real time qRT-PCR were as follows: CAVI: forward: 5'-CGCGACCCTAAACACCTCAA-3', reverse: 5'-GCCGTCAAAACTGTGTGCC-3' (63°C, 40 cycles); and Glyceraldehyde-3-phosphate dehydrogenase (GAPDH): forward: 5'-ACCACAGTCCATGCCATCAC-3', reverse: 5'-TCCACCACCC

Table I. Clinicopathological features.

	CRPC	Non-CRPC	p-Value*
Age, years mean±SD	68.7±7.7	66.2±5.2	0.18
PSA (ng/ml) mean±SD	41.8±28.4	8.8±4.1	<0.001
Gleason grade n (%)			
Low≤6	2 (5.6)	4 (18.2)	0.045
Intermediate=7	8 (22.2)	9 (40.9)	
High≥8	25 (72.2)	9 (40.9)	
T-grade n (%)			
Low≤T2	7 (19.4)	13 (59.1)	<0.004
High≥T3	29 (80.6)	9 (40.9)	
N n (%)			
Negative	16 (44.4)	22 (100)	<0.001
Positive	20 (55.6)	0 (0)	
M n (%)			
Negative	7 (19.4)	22 (100)	<0.001
Positive	29 (80.6)	0 (0)	
Plasma CAVI (ng/ml) mean±SD	1.46±1.37	0.56±0.32	<0.004
Total	36	22	

PSA: Prostate-specific antigen; CAVI: caveolin-1; M: metastasis. based on Student's t-test and Pearson's  $\chi^2$  test.

TGTTGCTGTA-3' (63°C, 40 cycles). For real-time qRT-PCR, transcripts were quantified using Applied Biosystems 7300 Real-Time PCR System (Life Technologies, Carlsbad, CA, USA) and Thunderbird SYBR qPCR Mix (ToYoBo, Tokyo, Japan). Experiments were repeated at least three times in triplicate; GAPDH was used as an internal control.

**Statistical analysis.** Statistical analysis was performed using the R i386 2.15.1 software package (Wirtschaftsuniversität Wien, Vienna University of Economics and Business, Vienna, Austria). The significance of differences in plasma CAVI levels among CRPC and non-CRPC patients were determined by Student's t-tests.  $p < 0.05$  was considered statistically significant.

## Results

**Patients' backgrounds and plasma CAVI levels.** Clinicopathological characteristics of patients with CRPC and non-CRPC are summarized in Table I. The mean ages (in years) of patients in the CRPC and non-CRPC groups were 68.3±7.4 (range=61-75) years and 66.9±8.3 (range=59-75) years, respectively. There were no significant differences between the two groups in terms of mean age distribution ( $p=0.18$ ). The mean serum prostate-specific antigen (PSA) levels of the CRPC and non-CRPC groups differed significantly (41.8±28.4 ng/ml and 8.8±4.1 ng/ml, respectively;  $p < 0.001$ ). In addition, patients in CRPC and non-CRPC groups differed significantly in clinicopathological characteristics such as Gleason grade, T grade and metastasis (extent, lymph node and bone) (Table I). Mean plasma CAVI

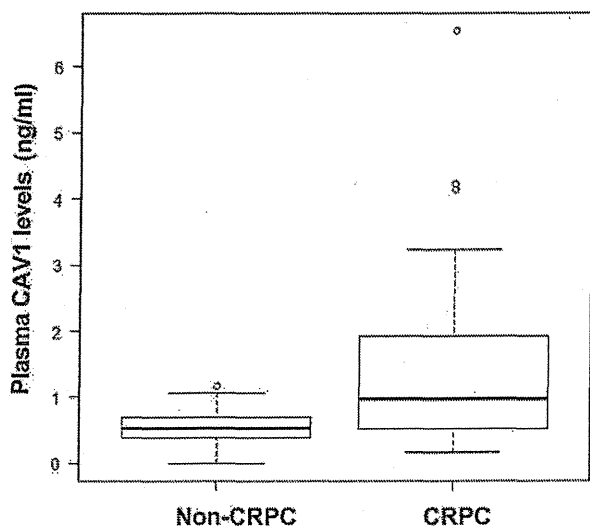


Figure 1. Plasma Caveolin-1 (CAV1) levels (ng/ml). Plasma CAV1 levels were significantly higher in the CRPC group ( $1.46 \pm 1.37$  ng/ml;  $n=36$ ) than in the non-CRPC group ( $0.56 \pm 0.32$  ng/ml;  $n=22$ ,  $p < 0.004$ ). Boxplot; The boundary of the box closest to zero indicates the 25th percentile, a line within the box marks the median, and the boundary of the box farthest from zero indicates the 75th percentile. Error bars above and below the boxes indicate the 90th and 10th percentiles, respectively.

levels in the CRPC group were much higher than in the non-CRPC group (CRPC= $1.46 \pm 1.37$  ng/ml, non-CRPC= $0.56 \pm 0.32$  ng/ml;  $p < 0.004$ ; Figure 1).

**Western blot analysis.** Western blot showed a single immunoreactive band for the CAV1 protein expression at 22 kDa. The loading control,  $\beta$ -Actin at 42 kDa, confirmed that there was equal protein loading (Figure 2). Western blot analysis showed that CAV1 expression was significantly greater in PC3 cells than in LNCaP cells.

**Real-time qRT-PCR.** Real-time qRT-PCR was performed by prostate cancer cells to examine the CAV1 mRNA expression, which was found to be significantly greater in PC3 cells than in LNCaP cells (CAV1/GAPDH, PC3 vs. LNCaP=1 vs. 0.002;  $p < 0.001$ ).

## Discussion

This study investigated whether CAV1 expression varied between Japanese patients with CRPC and in patients with androgen-sensitive prostate cancer. We also investigated differences in CAV1 protein and mRNA expression between PC3 cells (CRPC model) and LNCaP cells (non-CRPC model). Our data showed increasing levels of plasma CAV1 to have prognostic potential for prostate cancer progression.

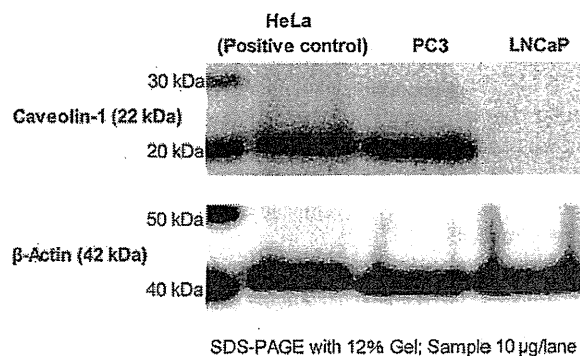


Figure 2. Western blot analysis showed significantly greater expression of Caveolin-1 (CAV1) in PC3 cells than in LNCaP cells.

CAV1 has been linked with various types of cancers over the past decade, during which it was most extensively studied in breast and prostate cancer. It was found that CAV1 levels in tumor tissue and in plasma may be associated with tumor protection or progression (10). In prostate cancer, in particular, elevated CAV1 expression was observed in tumor tissues in humans and in a mouse model, compared to non-tumor tissues (11-13). Another study implied that CAV1 and cancer-promoting growth factors collaborate in prostate cancer progression, although more evidence is needed (14). CAV1 is thought to suppress tumor growth and metastasis in human breast and colon cancer (15, 16). However, CAV1 function may differ among different organs, and CAV1 could thus exert opposing effects, resulting in promotion or suppression of tumor progression. For example, CAV1 expression increased in tumor samples from the kidney, prostate and stomach, and re-expression has been found in some advanced adenocarcinomas (17). Elevated CAV1 expression is associated with progression of some adenocarcinomas, such as prostate carcinoma (18), and in adult T-cell leukemia (19). Interestingly, activated CAV1 expression is associated with higher grades of prostate cancer, although few significant relationships have been identified between CAV1 expression and tumor multiplicity, recurrence, progression, or overall survival (16).

Li et al. showed that CAV1 was secreted by mouse and human prostate cancer cell lines, and that secreted CAV1 promoted cancer cell survival and clonal growth *in vitro* (20, 21). They further showed that tumor cell-secreted CAV1 promoted pro-angiogenic activities in prostate cancer through the phosphoinositol-3-kinase (PI3K)-protein kinase B (AKT)-endothelial nitric oxide synthase (eNOS) signaling pathway (22). Regarding the mechanisms through which CAV1 mediates oncogenic activities, they showed CAV1 to hold AKT in an activated form in prostate cancer cells by



binding to and inhibiting the serine/threonine protein phosphatases PP1 and PP2A (14). Thus, engagement of CAV1 as a tumor metastasis promoter depends on the cellular context, and at the molecular level, by the signaling molecules and signaling pathways affected and regulated by CAV1. We hypothesize that altered CAV1 expression interferes with homeostasis, and increases the frequency of prostate cancer.

Our results also show that CAV1 is associated with tumor progression and metastasis, and is distinctly elevated in androgen-resistant tumors. Therefore, CAV1 could be a marker for an aggressive form of cancer (18, 22, 23-27).

Suppression of CAV1 expression has been shown to restore sensitivity to androgens in androgen-insensitive tumors (13). Our findings, together with data from other studies, suggest that CAV1 is involved in disease pathogenesis and progression. Further study of its role in prostate cancer can contribute to the understanding of this disease, and possibly offer novel targeted therapeutic approaches. Although associations between CAV1 and high-risk tumors were identified in this study, we still cannot confirm CAV1 to be a marker for high-risk aggressive tumors, even at the phase when tumors are localized in the prostate and thus are still curable. To do so would require monitoring CAV1 levels in a follow-up study over the course of prostate cancer progression from its initial stages. Our results should also be verified in a larger group of patients, including those with disseminated disease.

### Conflicts of Interest

The Authors have no potential conflicts of interest.

### References

- Committee for Establishment of the Guidelines on Screening for Prostate Cancer. Japanese Urological Association: Updated Japanese Urological Association Guidelines on prostate-specific antigen-based screening for prostate cancer in 2010. *Int J Urol* 17(10): 830-838, 2010.
- Shaul PW and Anderson RG: Role of plasmalemmal caveolae in signal transduction. *Am J Physiol* 275: L843-L851, 1998.
- Williams TM and Lisanti MP: Caveolin-1 in oncogenic transformation, cancer, and metastasis. *Am J Physiol* 288: C494-C506, 2005.
- Cavallo-Medved D, Mai J, Donescu J, Sameni M and Sloane BF: Caveolin-1 mediates the expression and localization of cathepsin B, pro-urokinase plasminogen activator and their cell-surface receptors in human colorectal carcinoma cells. *J Cell Sci* 118: 1493-1503, 2005.
- Woodman SE, Ashton AW, Schubert W, Lee H, Williams TM, Medina FA, Wyckoff JB, Combs TP and Lisanti MP: Caveolin-1 knockout mice show an impaired angiogenic response to exogenous stimuli. *Am J Pathol* 162: 2059-2068, 2003.
- Wiechen K, Diatchenko L, Agoulnik A, Scharff KM, Schober H, Arlt K, Zhumabayeva B, Siebert PD, Diemel M, Schafer R and Sers C: Caveolin-1 is down-regulated in human ovarian carcinoma and acts as a candidate tumor suppressor gene. *Am J Pathol* 159: 1635-1643, 2001.
- Zhang H, Su L, Muller S, Tighiouart M, Xu Z, Zhang X, Shin HJ, Hunt J, Sun SY, Shin DM and Chen ZG: Restoration of caveolin-1 expression suppresses growth and metastasis of head and neck squamous cell carcinoma. *Br J Cancer* 99: 1684-1694, 2008.
- Karam JA, Lotan Y, Roehrborn CG, Ashfaq R, Karakiewicz PI and Shariat SF: Caveolin-1 overexpression is associated with aggressive prostate cancer recurrence. *Prostate* 67: 614-622, 2007.
- Zhang ZB, Cai L, Zheng SG, Xiong Y and Dong JH: Overexpression of caveolin-1 in hepatocellular carcinoma with metastasis and worse prognosis: correlation with vascular endothelial growth factor, microvessel density and unpaired artery. *Pathol Oncol Res* 15: 495-502, 2009.
- Williams TM and Lisanti MP: Caveolin-1 in oncogenic transformation, cancer, and metastasis. *Am J Physiol Cell Physiol* 288: C494-C506, 2005.
- Tahir SA, Ren CZ, Timme TL, Gdor Y, Hoogveen R, Morrisett JD, Frolow A, Ayala G, Wheeler TM and Thompson TC: Development of an immunoassay for serum caveolin-1: A novel biomarker for prostate cancer. *Clin Cancer Res* 9: 3653-3659, 2003.
- Nasu Y, Timme TL, Yang G, Bangma CH, Li L, Ren C, Park SH, DeLeon M, Wang J and Thompson TC: Suppression of caveolin expression induces androgen sensitivity in metastatic androgen-insensitive mouse prostate cancer cells. *Nat Med* 4: 1062-1064, 1998.
- Yang G, Truong LD, Wheeler TM and Thompson TC: Caveolin-1 expression in clinically confined human prostate cancer: A novel prognostic marker. *Cancer Res* 59: 5719-5723, 1999.
- Li L, Ren C, Yang G, Goltsov AA, Tabata K and Thompson TC: Caveolin-1 promotes autoregulatory, Akt-mediated induction of cancer-promoting growth factors in prostate cancer cells. *Mol Cancer Res* 7: 1781-1791, 2009.
- Lee SW, Reimer CL, Oh P, Campbell DB and Schnitzer JE: Tumor cell growth inhibition by caveolin re-expression in human breast cancer cells. *Oncogene* 16: 1391-1397, 1998.
- Rajjayabun PH, Garg S, Durkan GC, Charlton R, Robinson MC and Mellon JK: Caveolin-1 expression is associated with high-grade bladder cancer. *Urology* 58: 811-814, 2001.
- Wiechen K, Sers C, Agoulnik A, Arlt K, Diemel M, Schlag PM and Schneider U: Down-regulation of caveolin-1, a candidate tumor suppressor gene, in sarcomas. *Am J Pathol* 158: 833-839, 2001.
- Thompson TC, Tahir SA, Li L, Watanabe M, Naruishi K, Yang G, Kadmon D, Logothetis CJ, Troncoso P, Ren C, Goltsov A and Park S: The role of caveolin-1 in prostate cancer: clinical implications. *Prostate Cancer Prostatic Dis* 13(1): 6-11, 2010.
- Sawada S, Ishikawa C, Tanji H, Nakachi S, Senba M, Okudaira T, Uchihara JN, Taira N, Ohshiro K, Yamada Y, Tanaka Y, Uezato H, Ohshima K, Sasai K, Burgering BM, Duc Dodon M, Fujii M, Sunakawa H and Mori N: Overexpression of caveolin-1 in adult T-cell leukemia. *Blood* 115: 2220-2230, 2010.
- Li L, Ren CH, Tahir SA, Ren C and Thompson TC: Caveolin-1 maintains activated AKT in prostate cancer cells through scaffolding domain binding site interactions with and inhibition of serine/threonine protein phosphatases PP1 and PP2A. *Mol Cell Biol* 23: 9389-9404, 2003.

- 21 Li L, Yang G, Ebara S, Satoh T, Nasu Y, Timme TL, Ren C, Wang J, Tahir SA and Thompson TC: Caveolin-1 mediates testosterone-stimulated survival/clonal growth and promotes metastatic activities in prostate cancer cells. *Cancer Res* 61: 4386-92, 2001.
- 22 Tahir SA, Yang G, Ebara S, Timme TL, Satoh T, Li L, Goltsov A, Ittmann M, Morrisett JD and Thompson TC: Secreted caveolin-1 stimulates cell survival/clonal growth and contributes to metastasis in androgen-insensitive prostate cancer. *Cancer Res* 61: 3882-3885, 2001.
- 23 Watanabe M, Yang G, Cao GW, Tahir SA, Naruishi K, Tabata K, Fattah EA, Rajagopalan K, Timme TL, Park S, Kurosaka S, Edamura K, Tanimoto R, Demayo FJ, Goltsov AA and Thompson TC: Functional analysis of secreted caveolin-1 in mouse models of prostate cancer progression. *Mol Cancer Res* 7: 1446-1455, 2009.
- 24 Tahir SA, Yang G, Ebara S, Timme TL, Satoh T, Li L, Goltsov A, Ittmann M, Morrisett JD and Thompson TC: Secreted caveolin-1 stimulates cell survival/clonal growth and contributes to metastasis in androgen-insensitive prostate cancer. *Cancer Res* 61: 3882-3885, 2001.
- 25 Yang G, Truong LD, Timme TL, Ren C, Wheeler TM, Park SH, Nasu Y, Bangma CH, Kattan MW, Scardino PT and Thompson TC: Elevated expression of caveolin is associated with prostate and breast cancer. *Clin Cancer Res* 4: 1873-1880, 1998.
- 26 Thompson TC, Timme TL, Li L and Goltsov A: Caveolin-1, a metastasis-related gene that promotes cell survival in prostate cancer. *Apoptosis* 4: 233-237, 1999.
- 27 Mouraviev V, Li LK, Tahir SA, Yang G, Timme TM, Goltsov A, Ren C, Satoh T, Wheeler TM, Ittmann MM, Miles BJ, Amato RJ, Kadmon D and Thompson TC: The role of caveolin-1 in androgen insensitive prostate cancer. *J Urol* 168: 1589-1596, 2002.

*Received February 28, 2013*

*Revised March 28, 2013*

*Accepted March 29, 2013*

SHORT COMMUNICATION

## Genistein induces apoptotic cell death associated with inhibition of the NF- $\kappa$ B pathway in adult T-cell leukemia cells

Masao Yamasaki<sup>1</sup>, Yoshihiro Mine<sup>1</sup>, Misato Nishimura<sup>1</sup>, Satoshi Fujita<sup>1</sup>, Yoichi Sakakibara<sup>1</sup>, Masahito Suiko<sup>1</sup>, Kazuhiro Morishita<sup>2</sup> and Kazuo Nishiyama<sup>1\*</sup>

<sup>1</sup> Faculty of Agriculture, Department of Biochemistry and Applied Biosciences, University of Miyazaki, 1-1 Gakuenkibanadai-nishi, Miyazaki 889-2192, Japan

<sup>2</sup> Faculty of Medicine, Department of Biochemistry, University of Miyazaki, 5200 Kihara Kiyotake, Miyazaki 889-1692, Japan

### Abstract

We have shown that genistein inhibits the growth of adult T-cell leukemia (ATL) cells in vitro and in vivo, and this leads to pronounced G2/M arrest. This report shows that genistein induces apoptotic death in ATL cells. Although the pan-caspase inhibitor, Z-VAD-fmk, did not inhibit genistein-induced apoptosis, release of apoptosis-inducing factor (AIF) into the cytosol occurred. Poly-ADP ribose polymerase inhibition also abrogated genistein-induced apoptosis. Genistein decreased nuclear p65 translocation and I $\kappa$ B $\alpha$  phosphorylation, and downregulated the anti-apoptotic proteins, XIAP, cIAP and survivin, NF- $\kappa$ B-responsive gene products. Thus, genistein is a promising agent for ATL that induces caspase-independent apoptosis through inhibition of the NF- $\kappa$ B pathway.

**Keywords:** adult T-cell leukemia; apoptosis inducing factor; caspase; genistein; isoflavone; NF- $\kappa$ B pathway

### Introduction

Southwestern Kyushu in Japan is known for its high prevalence of human T-lymphotropic virus type I (HTLV-I). HTLV-I is the etiologic agent of the CD4<sup>+</sup> T-cell malignancy adult T-cell leukemia (ATL). Therefore, ATL is designated as an endemic disease particularly in certain pockets of the Japanese population. Among infected individuals, only 1–5% develop ATL, and it is well established that this process requires 20–50 years after HTLV-I infection. ATL is categorised into four types according to its clinical phenotypes: acute, chronic, smoldering and lymphoma. The acute type constitutes 55–75% of all ATL cases (Hanchard et al., 1990; Yamaguchi et al., 1990). Acute ATL is aggressively malignant and fatal, as it is accompanied by pulmonary complications, opportunistic infections and uncontrolled hypercalcemia. Aggressive forms of ATL are resistant to conventional chemotherapy. Therefore, it is important to identify appropriate therapeutic methods to prevent the development of ATL or prolong survival after its occurrence.

Local cofactors, such as food culture, play an important role in ATL occurrence. In Japan in particular, ATL develops ~50 years after infection, which is comparatively longer than in other areas of the world. Some components from natural foods, for example as curcumin, capsaicin and fucoidan, are effective in ATL treatment (Zhang et al., 2003; Haneji et al., 2005; Tomita et al., 2006a, b). Soybean isoflavone inhibits the proliferation or induces cell death in different types of cancers, including those involving non-ATL leukemia cells (Hewitt and Singletary, 2003; Su et al., 2003; Chang et al., 2004; Liao et al., 2004). We previously showed that soy isoflavones potently inhibited the proliferation of ATL cells in vitro and in vivo (Yamasaki et al., 2007). Genistein demonstrated a striking ability to induce the accumulation of p53 protein and stimulate its phosphorylation at ser-15, 20 and 37 in ATL cells. This effect was accompanied by growth inhibition and G2/M arrest. Genistein also induced cell death in ATL cells, but the molecular mechanisms remain unclear. Here, we have examined the apoptosis inducing activity and role of the NF- $\kappa$ B pathway in the cytotoxic effect of genistein on ATL cells.

\*Corresponding author: e-mail: nishiyam@cc.miyazaki-u.ac.jp

**Abbreviations:** HTLV-I, human T-lymphotropic virus type I; ATL, adult T-cell leukemia; TSP/HAM, tropical spastic paraparesis/HTLV-I-associated myelopathy; TTBS, Tris-buffered saline with 0.1% Tween-20; PBS, phosphate-buffered saline; PFT, pifithrin- $\alpha$ ; 3-AB, 3-aminobenzamide; PARP, poly-ADP ribose polymerase; AIF, apoptosis-inducing factor; cIAP-2, cellular inhibitor of apoptosis protein-2; XIAP, X-linked inhibitor of apoptosis protein

## Materials and methods

### Materials

Genistein was obtained from Fujicco (Kobe, Japan). 3-Aminobenzamide (3-AB) (Enzo Life Sciences), Z-VAD-fmk (Peptide Institute, Osaka, Japan) and Bay11-7082 (Cayman Chemical, Ann Arbor, MI) were used to inhibit poly-ADP ribose polymerase (PARP), pan-caspase and I $\kappa$ B- $\alpha$  respectively. Peroxidase-conjugated anti-mouse IgG, peroxidase-conjugated anti-rabbit IgG and anti-COX4 were obtained from Santa Cruz Biotechnology, Santa Cruz, CA). Anti- $\beta$ -actin clone AC-15 was obtained from Sigma (St. Louis, MO); anti-histone H1 was obtained from Acris Antibodies (Herford, Germany), and other antibodies (against NF- $\kappa$ B p65, phosphorylated I $\kappa$ B $\alpha$ , I $\kappa$ B $\alpha$ , apoptosis-inducing factor (AIF), cellular inhibitor of apoptosis protein-2 (cIAP-2), X-linked inhibitor of apoptosis protein (XIAP) and survivin were purchased from Cell Signaling Technology (Beverly, MA).

### Cell culture

Hut102 cells provided by Hayashibara Biochemical Laboratories, Inc. (Okayama, Japan) were maintained in RPMI1640 medium supplemented with 10% fetal bovine serum containing 100 units/mL penicillin G and 100  $\mu$ g/mL streptomycin. The cells were subcultured twice a week. For experiments, the cells were adjusted to  $1 \times 10^5$  per mL and cultured with 0–30  $\mu$ M isoflavones for 24 and 48 h.

### Cell cycle analysis

The cells were fixed in ice-cold methanol for 30 min before treatment with 10  $\mu$ g/mL propidium iodide and 10  $\mu$ g/mL RNase. Cycle analysis involved a Coulter, Epics XL flow cytometer (Beckman Coulter, Inc., Fullerton, CA) equipped with MultiCycle software (San Diego, CA).

### Annexin-V staining

Annexin-V positive cells were identified using a commercial kit (Bender MedSystems, Vienna, Austria). After staining, the ratio of annexin-V positive cells among all cells was detected by flow cytometry.

### Western blot analysis

At the end of the culture period, cells were lysed in 50 mM Tris-HCl (pH 7.5) containing 150 mM NaCl, 2% Triton X-100, 2 mM EDTA, 50 mM NaF, 30 mM Na<sub>4</sub>P<sub>2</sub>O<sub>7</sub> and 1/50 volume protease inhibitor cocktail (Nacalai Tesque, Kyoto, Japan) for the analysis of total cell lysate. Nuclear and cytoplasmic extracts were separated and prepared using the NE-PER Nuclear and Cytoplasmic Extraction Reagents

(Pierce, Rockford, IL). For the detection of cytosolic AIF, cells were treated with ice-cold cytosol recovery buffer (0.025% digitonin, 5 mM MgCl<sub>2</sub>, 1 mM EDTA, 10 mM KCl, 250 mM sucrose, 25 mM NaF, 1 mM sodium orthovanadate/20 mM HEPES-KOH at pH 7.2) for 5 min. After centrifugation at 8,500g for 5 min, the supernatant was used as cytosolic fraction. Protein concentration was measured using the BCA protein assay reagent (Pierce). Lysates containing 10  $\mu$ g of protein were separated by electrophoresis on a 10% SDS-polyacrylamide gel and transferred to PVDF Hybond-P membrane (Amersham-Pharmacia Biotech, Buckinghamshire, UK). Blocking used 5% defatted milk or 5% bovine serum albumin fraction V (for the detection of phosphorylated protein) in Tris-buffered saline with 0.1% Tween-20 (TTBS). Antibodies were diluted in Can Get Signal solutions 1 and 2 (Toyobo, Tokyo, Japan). The membrane was washed with TTBS after each antibody binding reaction. Detection of each protein was performed using the ECL Plus kit (Amersham Pharmacia). The band intensity was quantified using the Image J software and data shown are representative blot patterns. Mean values were determined for at least three independent experiments.

### Statistical analysis

Data were analysed using Student's *t*-test and the Tukey-Kramer test to evaluate the significance of differences. Significance was defined as  $P < 0.05$ .

## Results

### Genistein inhibits growth and induces apoptosis of ATL cells

Genistein strongly inhibited the growth of ATL cells in vitro and in vivo, as previously known (Figure 1A). In particular, 30  $\mu$ M genistein completely inhibited the growth of Hut102 cells at 24, 48 and 72 h, inducing the accumulation of the G2/M population (Figure 1B). At 10  $\mu$ M, genistein significantly inhibited growth at 48 and 72 h, but did not increase the G2/M phase population. Genistein (30  $\mu$ M) significantly increased the su-G1 population and annexin V-positive cells at 48 h (Figures 1B and 1C), which suggest that cell cycle arrest and the induction of apoptotic cell death both contributed to the growth inhibition of ATL cells. The mitochondrial membrane potential was strongly impaired at 30  $\mu$ M treatment, but not by 10  $\mu$ M at 24 and 48 h (Figure 1D).

### Genistein induces caspase-independent apoptosis

To determine the molecular mechanism underlying genistein-induced apoptosis, cells were treated with Z-VAD-fmk

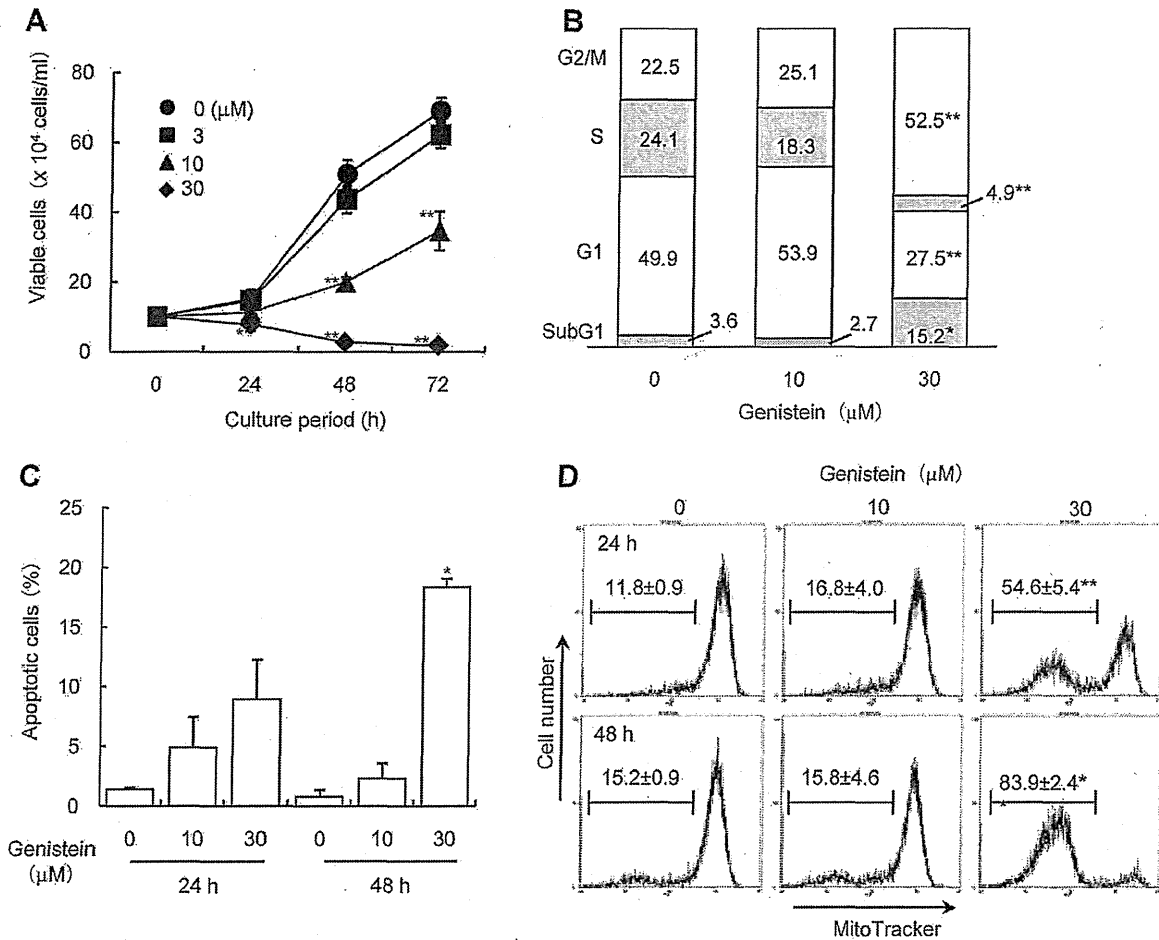


**Figure 1** Induction of apoptotic cell death and G2/M cell cycle arrest of Hut102 cells by genistein. (A) Cells were treated with 0, 3, 10 and 30 μM genistein for 24–72 h and viable cells were counted using the trypan blue dye exclusion method. (B) Cells were treated with 0, 10 and 30 μM genistein for 48 h and cell cycle analysis was performed. (C,D) Cells were treated with 0, 10 and 30 μM genistein for 24 or 48 h and the number of Annexin-V-positive cells (C) and the mitochondria membrane potential (D) were determined by flow cytometry. Data are shown as the mean ± SE of three independent experiments. Bars marked with asterisks are significant with respect to the control at \**P* < 0.05 and \*\*0.01.

to assess the involvement of a caspase-dependent pathway. Z-VAD-fmk had no effect on the number of viable cells (Figure 2A). Western blot analysis showed that genistein did not activate caspase-3 (data not shown), which implies the involvement of a caspase-independent pathway. Cytosolic AIF levels were increased by 30 μM genistein treatment for 24 h (Figure 2B). COX4, a mitochondrial marker protein, was not detected in cytosolic fraction, showing no contamination of mitochondrial protein into cytosolic fraction (Figure 2C). AIF release from mitochondria is known to be stimulated by poly-ADP ribose which is a product of PARP overactivation. Thus, the cells treated with 3-AB, inhibitor of PARP, and genistein showed that the former partially abrogated the cytotoxic activity of the latter (Figure 2D).

**Genistein decreases NF-κB activity**

Finally, the effect of genistein on the activity of NF-κB was examined. Although 30 μM genistein significantly reduced the number of viable cells and impaired the mitochondrial membrane potential after 24 h of treatment, nuclear p65 and phosphorylated IκBα levels were unchanged. However, the levels of nuclear p65 and phosphorylated IκBα decreased significantly after 48 h (Figure 3A). GAPDH was not detected in nuclear fraction, and a strong signal of histone H1 expression was detected in nuclear fraction (Figure 3B), showing no contamination of cytosol protein into nuclear fraction. Although this data indicate that cytosolic fraction contains histone H1, we did not use cytosolic fraction for analysis. NF-κB mediates the

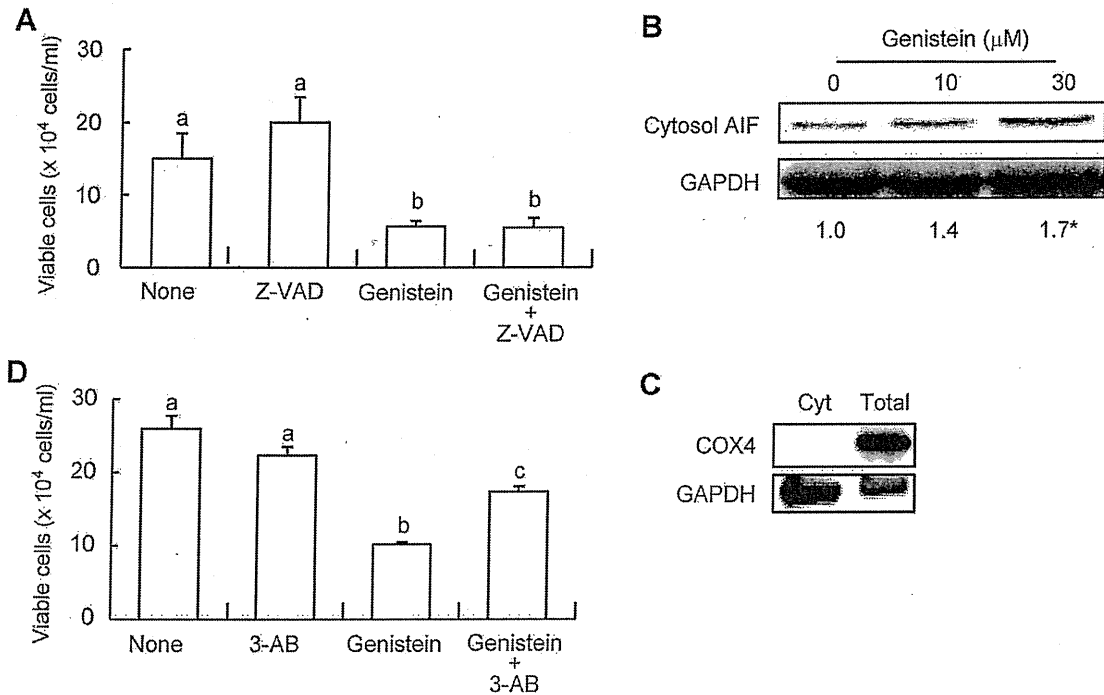


**Figure 2** Genistein induces caspase independent apoptosis. (A, C) Cells were treated with 0 and 30  $\mu\text{M}$  genistein with 0 and 20  $\mu\text{M}$  Z-VAD-frnk (A) or 0 and 20 mM 3-AB (D) for 24 h and viable cells were counted using the trypan blue dye exclusion method. (A) Cells were treated with 0, 10 and 30  $\mu\text{M}$  genistein for 24 h, and cytosolic AIF and GAPDH were then detected using Western blot analysis. Data in (A) and (D) are shown as means  $\pm$  SE of three independent experiments and the numbers in (B) show the mean values of the quantified band intensities for three independent experiments. The representative blot patterns are shown. Numbers marked with asterisks are significant with respect to the control at \* $P < 0.05$  and \*\* $P < 0.01$ . Values that do not sharing any alphabetic letters are significantly different from each other,  $P < 0.05$ . (C) COX4 and GAPDH detection in cytosolic fraction to confirm no contamination between subcellular fractions. Cyt, cytosolic fraction.

transcription of several anti-apoptotic proteins (Figure 3C). Bay11-7082 was used as a positive control for NF- $\kappa$ B inhibition. After 48 h treatment with 10 and 30  $\mu\text{M}$  genistein, the levels of cIAP-2, XIAP and survivin were significantly decreased.

## Discussion

Having shown that genistein strongly inhibits the growth of ATL cells in vitro and in vivo via G2/M cell cycle arrest (Figures 1A and 1B), we found that 30  $\mu\text{M}$  genistein significantly increased the sub-G1 population and the number of annexin V-positive cells, suggesting that cell cycle arrest and induction of apoptotic cell death both contribute to the growth inhibition of ATL cells. In contrast to extrinsic death signals, cellular stresses (DNA damage) induce an intrinsic apoptotic program regulated predominantly by the mitochondria. Because these stimuli induce permeabilisation of the mitochondrial outer membrane, the findings in Figures 1B–D suggest that genistein-induced mitochondria-mediated apoptosis in Hut102 cells. Soy-bean isoflavone induced apoptotic cell death in xenografted ATL cells in non-

obese diabetic/SCID/gammac null (NOG) mice (Yamasaki et al., 2007). Thus, mitochondria-mediated apoptotic cell death may be involved in the growth inhibitory effect of genistein on ATL cells.

Genistein can induce apoptotic cell death in different types of cells (Hewitt and Singletary, 2003; Su et al., 2003; Chang et al., 2004; Liao et al., 2004). It also induces caspase-dependent apoptosis in ALL, multiple myeloma cells and T-lymphoma cells (Baxa et al., 2005; Li et al., 2011). In contrast, our data show that caspase activation is dispensable for cell death, suggesting the importance of other apoptotic pathways. AIF is a caspase-independent death effect that is localised to the mitochondria under steady-state conditions, but translocates to the cytosol and nucleus under different apoptotic stimuli, including genistein administration (Karmakar et al., 2009; Mohan et al., 2009). Genistein induces translocation of AIF to the cytosolic fraction, which implies that AIF-mediated apoptotic cell death. PARP-1 activation and the resulting poly-ADP ribose (PAR) overproduction promotes to AIF translocation from mitochondria to nuclei (Yu et al., 2002, 2006). The PARP inhibitor, 3-AB, partially abrogated the cytotoxicity of